KUNS-2402
RIKEN-MP-49
YITP-12-46

Strong-coupling Analysis of Parity Phase Structure in Staggered-Wilson Fermions

Tatsuhiro Misumi*

Physics Department, Brookhaven National Laboratory, Upton, New York 11973, USA

Takashi Z. Nakano†

Department of Physics, Yukawa Institute for Theoretical Physics, Kyoto University, Kyoto 606-8502, Japan

Taro Kimura‡

Mathematical Physics Laboratory, RIKEN Nishina Center, Saitama 351-0198, Japan

Akira Ohnishi§

Yukawa Institute for Theoretical Physics, Kyoto University, Kyoto 606-8502, Japan

We study strong-coupling lattice QCD with staggered-Wilson fermions, with emphasis on discrete symmetries and possibility of their spontaneous breaking. We perform hopping parameter expansion and effective potential analyses in the strong-coupling limit. From gap equations we find nonzero pion condensate in some range of a mass parameter, which indicates existence of the parity-broken phase in lattice QCD with staggered-Wilson fermions. We also find massless pions and PCAC relations around second-order phase boundary. These results suggest that we can take a chiral limit by tuning a mass parameter in lattice QCD with staggered-Wilson fermions as with the Wilson fermion.

*Electronic address: tmisumi@bnl.gov
†Electronic address: tnakano@yukawa.kyoto-u.ac.jp
‡Electronic address: tkimura@ribf.riken.jp
§Electronic address: ohnishi@yukawa.kyoto-u.ac.jp

I. INTRODUCTION

Since the dawn of lattice field theory [1], the doubling problem of fermions has been a notorious obstacle to lattice simulations. Among several prescriptions for this problem, the Wilson fermion simply bypasses the no-go theorem [2] by introducing a species-splitting mass term into the naive lattice fermion. This Wilson term is regarded as one example of "flavored-mass terms" which split original 16 fermion species into plural branches [3, 4]. It has been recently shown that the flavored-mass terms can also be constructed for staggered fermions [5–7] in Ref. [8–10]. The original purpose of introducing these terms was establishment of the index theorem with staggered fermions [8]. A bonus here is that staggered fermions with the flavored-mass terms can be applied to lattice QCD simulations as Wilson fermion and an overlap kernel. One possible advantage of these novel formulations, called staggered-Wilson and staggered-overlap, is reduction of matrix sizes in the Dirac operators, which would lead to reduction of numerical costs in lattice simulations. The numerical advantage in the staggered-overlap fermion have been shown in [11]. Now further study is required toward lattice QCD with these lattice fermions.

The purpose of this work is to reveal properties of staggered-Wilson fermions in terms of the parity-phase structure (Aoki phase) [12–17]. As is well-known, the existence of the Aoki phase and the second-order phase boundary in Wilson-type fermions enables us to perform lattice QCD simulations by taking a chiral limit since the critical behavior near the phase boundary reproduces massless pions and the PCAC relation. Besides, understanding the phase structure also gives practical information for the application of the overlap [18, 19] and domain-wall [20, 21] versions, both built on the Wilson-type kernel. Thus, in order to judge applicability of these new lattice fermions, it is essential to investigate the Aoki phase in the staggered-Wilson fermions. The phase structure for the staggered-Wilson fermion was first studied by using the Gross-Neveu model in Ref. [22, 23] and the present paper shows further investigation of this topic.

In this paper, we investigate strong-coupling lattice QCD [24] with emphasis on parity-phase structure for two types of staggered-Wilson fermions [9, 10]. Firstly we discuss discrete symmetries of staggered-Wilson fermions, and show that physical parity and charge conjugation can be defined in both cases while hypercubic symmetry depends on types of staggered-Wilson fermions. Secondly, we perform hopping-parameter expansion and effec-

tive potential analysis for meson fields in the strong-coupling limit. For this purpose, we develop a method to derive the effective potential for lattice fermions with multiple-hopping terms. The gap equations show that pion condensate becomes non-zero in some range of a mass parameter, which indicates that parity-broken phase appears in this range. We also study meson masses around the second-order phase boundary, and find that massless pions and PCAC relations are reproduced. Lastly, we discuss parity-flavor symmetry breaking for 2-flavor cases. These results suggest that we can take a chiral limit by tuning a mass parameter in lattice QCD with staggered-Wilson fermions as with the Wilson fermion.

This paper is organized as follows. In Sec. II, we review staggered flavored-mass terms and two types of staggered-Wilson fermions. In Sec. III, we study discrete symmetries of staggered-Wilson fermions. In Sec. IV, we study hopping parameter expansion in lattice QCD with these fermions. In Sec. V, we investigate Aoki phase structure by effective potential analysis. In Sec. VI, we discuss parity-flavor symmetry breaking in two-flavor cases. In Sec. VII, we devote ourselves to a summary and discussion.

II. STAGGERED-WILSON FERMIONS

Before looking into staggered-Wilson fermions, we review the Wilson fermion and its relatives. The Wilson term splits 16 species of naive fermions into 5 branches with 1, 4, 6, 4 and 1 fermions. We call this kind of species-splitting terms "flavored-mass terms". As shown in [3], there are 4 types of flavored-mass terms for naive fermion which satisfy γ_5 hermiticity. (γ_5 in the naive fermion is flavored such as $\gamma_5 \otimes (\tau_3 \otimes \tau_3 \otimes \tau_3 \otimes \tau_3)$ in the spin-flavor representation.) All these terms with proper mass shifts lead to a second derivative term as $\sim a \int dx^4 \bar{\psi} D_\mu^2 \psi$ up to $\mathcal{O}(a^2)$ errors. Thus we can regard them as cousins of Wilson fermion.

There are also non-trivial flavored-mass terms for staggered fermions, which split 4 tastes into branches and satisfy γ_5 hermiticity. Since γ_5 is expressed in spin-taste representation as $\gamma_5 \otimes \gamma_5$ in this case, we only have two flavored-mass terms satisfying γ_5 hermiticity: $\mathbf{1} \otimes \gamma_5$ and $\mathbf{1} \otimes \sigma_{\mu\nu}$. (For larger discrete symmetry one needs to take a proper sum for μ, ν in the latter case.) These spin-flavor representations translate into four- and two-hopping terms in

the one-component staggered action up to $\mathcal{O}(a)$ errors. The first type is given by

$$M_A = \epsilon \sum_{sym} \eta_1\eta_2\eta_3\eta_4 C_1C_2C_3C_4 = (\mathbf{1}\otimes\gamma_5) + \mathcal{O}(a) \ , \tag{1}$$

with

$$(\epsilon)_{xy} = (-1)^{x_1+\ldots+x_4}\delta_{x,y} \ , \tag{2}$$

$$(\eta_\mu)_{xy} = (-1)^{x_1+\ldots+x_{\mu-1}}\delta_{x,y} \ , \tag{3}$$

$$C_\mu = (V_\mu + V_\mu^\dagger)/2 \ , \tag{4}$$

$$(V_\mu)_{xy} = U_{\mu,x}\delta_{y,x+\mu} \ . \tag{5}$$

The second type is given by

$$\begin{aligned} M_H &= \frac{i}{\sqrt{3}}(\eta_{12}C_{12} + \eta_{34}C_{34} + \eta_{13}C_{13} + \eta_{42}C_{42} + \eta_{14}C_{14} + \eta_{23}C_{23}) \ , \\ &= [\mathbf{1}\otimes(\sigma_{12}+\sigma_{34}+\sigma_{13}+\sigma_{42}+\sigma_{14}+\sigma_{23})] + \mathcal{O}(a) \ , \end{aligned} \tag{6}$$

with

$$(\eta_{\mu\nu})_{xy} = \epsilon_{\mu\nu}\eta_\mu\eta_\nu\delta_{x,y} \ , \tag{7}$$

$$(\epsilon_{\mu\nu})_{xy} = (-1)^{x_\mu+x_\nu}\delta_{x,y} \ , \tag{8}$$

$$C_{\mu\nu} = (C_\mu C_\nu + C_\nu C_\mu)/2 \ . \tag{9}$$

We refer to M_A and M_H as the Adams- [8] and Hoelbling-type [10], respectively. The former splits the 4 tastes into two branches with positive mass and the other two with negative mass. These two branches correspond to $+1$ and -1 eigenvalues of γ_5 in the taste space. The latter splits them into one with positive mass, two with zero mass and the other one with negative mass. We note that M_A and M_H are also derived from the flavored mass terms for naive fermions through spin-diagonalization as shown in [3]. Now we introduce a Wilson parameter $r = r\delta_{x,y}$ and shift mass as in Wilson fermions [10]. Then the Adams-type staggered-Wilson fermion action is given by

$$S_{\rm A} \ = \ \sum_{xy} \bar{\chi}_x[\eta_\mu D_\mu + r(1+M_A) + M]_{xy}\chi_y \ , \tag{10}$$

$$D_\mu = \frac{1}{2}(V_\mu - V_\mu^\dagger) \ . \tag{11}$$

Here M stands for the usual taste-singlet mass ($M = M\delta_{x,y}$). The Hoelbling-type fermion action is given by

$$S_{\rm H} = \sum_{xy} \bar{\chi}_x [\eta_\mu D_\mu + r(2 + M_H) + M]_{xy} \chi_y \ . \tag{12}$$

It is obvious that these lattice fermions have possibility to be two- or one-flavor Wilson fermions. In lattice QCD simulation with these fermions, the mass parameter M will be tuned to take a chiral limit as Wilson fermions. For some negative value of the mass parameter: $-1 < M < 0$ for Adams-type and $-2 < M < 0$ for Hoelbling-type, we obtain two-flavor and one-flavor overlap fermions respectively by using the overlap formula in principle.

III. DISCRETE SYMMETRIES

In this section, we discuss discrete symmetry of staggered-Wilson fermions. A potential problem with staggered-Wilson fermions in lattice QCD is discrete symmetry breaking. As discussed in [9, 10], the discrete symmetry possessed by the original staggered fermion is broken to its subgroup both in the Adams-type and Hoelbling-type actions. We below list all the staggered discrete symmetries (shift, axis reversal, rotation and charge conjugation), and look into their status in staggered-Wilson fermions. Shift transformation is given by

$$\mathcal{S}_\mu : \ \chi_x \to \zeta_\mu(x) \chi_{x+\hat{\mu}}, \quad \bar{\chi}_x \to \zeta_\mu(x) \bar{\chi}_{x+\hat{\mu}}, \quad U_{\nu,x} \to U_{\nu,x+\hat{\mu}} \ , \tag{13}$$

with $\zeta_1(x) = (-1)^{x_2+x_3+x_4}$, $\zeta_2(x) = (-1)^{x_3+x_4}$, $\zeta_3(x) = (-1)^{x_4}$ and $\zeta_4(x) = 1$. It is obvious that this transformation flips the sign of both flavored-mass terms. The Adams type is invariant under the two-shift subgroup as $x \to x + \hat{1} \pm \hat{\mu}$ while the Hoelbling type is invariant under four-shift subgroup as $x \to x + \hat{1} \pm \hat{2} \pm \hat{3} \pm \hat{4}$. Note that these subgroups include the doubled shift $x \to x + 2\hat{\mu}$ as their subgroup. The axis reversal transformation is given by,

$$\mathcal{I}_\mu : \ \chi_x \to (-1)^{x_\mu} \chi_{Ix}, \quad \bar{\chi}_x \to (-1)^{x_\mu} \bar{\chi}_{Ix}, \quad U_{\nu,x} \to U_{\nu,Ix} \ , \tag{14}$$

with $I = I^\mu$ is the axis reversal $x_\mu \to -x_\mu$, $x_\rho \to x_\rho$, $\rho \neq \mu$. It again flips the sign of the flavored-mass terms. The staggered rotational transformation is given by

$$\mathcal{R}_{\rho\sigma} : \ \chi_x \to S_R(R^{-1}x) \chi_{R^{-1}x}, \quad \bar{\chi}_x \to S_R(R^{-1}x) \bar{\chi}_{R^{-1}x}, \quad U_{\nu,x} \to U_{\nu,Rx} \ , \tag{15}$$

where $R_{\rho\sigma}$ is the rotation $x_\rho \to x_\sigma$, $x_\sigma \to -x_\rho$, $x_\tau \to x_\tau$, $\tau \neq \rho, \sigma$ and $S_R(x) = \frac{1}{2}[1 \pm \eta_\rho(x)\eta_\sigma(x) \mp \zeta_\rho(x)\zeta_\sigma(x) + \eta_\rho(x)\eta_\sigma(x)\zeta_\rho(x)\zeta_\sigma(x)]$ with $\rho \lesseqgtr \sigma$. It is notable that the Adams-type fermion keeps this staggered rotation symmetry while the Hoelbling type loses it. The staggered charge conjugation transformation is given by

$$\mathcal{C}: \ \chi_x \to \epsilon_x \bar{\chi}_x^T, \quad \bar{\chi}_x \to -\epsilon_x \chi_x^T, \quad U_{\nu,x} \to U_{\nu,x}^* \ . \tag{16}$$

The Adams-type fermion keeps this symmetry while the Hoelbling type loses it.

We next elucidate residual subgroups possessed by staggered-Wilson fermions, and discuss how to define physical discrete symmetries as Parity, Charge conjugation and Hypercubic symmetry. For this purpose we separate spin and flavor rotations in the above transformations. Here we utilize the momentum-space representation in [25, 26]. In this representation we can define two set of clifford generators Γ_μ and Ξ_μ, which operate on spinor and flavor spaces in the momentum-space field $\phi(p)$, respectively. (Details are shown in Appendix. A.) Then the shift transformation translates into

$$\mathcal{S}_\mu: \ \phi(p) \ \to \ \exp(ip_\mu)\Xi_\mu \, \phi(p) \ . \tag{17}$$

The axis reversal translates into

$$\mathcal{I}_\mu : \phi(p) \ \to \ \Gamma_\mu \Gamma_5 \Xi_\mu \Xi_5 \, \phi(Ip) \ . \tag{18}$$

The rotational transformation translates into

$$\mathcal{R}_{\rho\sigma}: \ \phi(p) \ \to \ \exp(\frac{\pi}{4}\Gamma_\rho\Gamma_\sigma) \exp(\frac{\pi}{4}\Xi_\rho\Xi_\sigma) \, \phi(R^{-1}p) \ . \tag{19}$$

By using this representation we figure out residual discrete symmetries of staggered-Wilson fermions as follows. We first consider parity. Both staggered-Wilson fermions are invariant under

$$\mathcal{I}_s\mathcal{S}_4 \sim \exp(ip_4)\Gamma_1\Gamma_2\Gamma_3\Gamma_5 \, \phi(-\mathbf{p}, p_4) \sim \exp(ip_4)\Gamma_4 \, \phi(-\mathbf{p}, p_4) \ , \tag{20}$$

with $\mathcal{I}_s \equiv \mathcal{I}_1\mathcal{I}_2\mathcal{I}_3$. This is essentially the continuum parity transformation [26]. In the continuum limit the phase factor disappears and it results in the continuum parity transformations $P : \psi(p) \to \gamma_4\psi(-\mathbf{p}, p_4)$ for the Dirac fermion. We thus conclude both staggered-Wilson fermions possess symmetry leading to physical parity symmetry P. We note the simple combination of μ-shift and μ-axis reversal (shifted-axis reversal:$\mathcal{S}_\mu\mathcal{I}_\mu$) is also a symmetry of both fermions.

We next consider physical charge conjugation. In the case of Adams fermion the staggered charge conjugation symmetry $\mathcal{C}$ in Eq. (16) remains intact. Thus, physical charge conjugation for the two-flavor branch can be formed in a similar way to usual staggered fermions as shown in [26] ($C \sim \mathcal{C}\mathcal{S}_2\mathcal{S}_4\mathcal{I}_2\mathcal{I}_4$). On the other hand, the Hoelbling type breaks $\mathcal{C}$. In this case, however, we can define another charge conjugation by combining $\mathcal{C}$ with rotation transformation as

$$\mathcal{C}_T : \ \mathcal{R}_{21}\mathcal{R}_{13}^2\mathcal{C} \ . \tag{21}$$

The Hoelbling action is invariant under this transformation. By using this symmetry we can define physical charge conjugation C for one-flavor branch as in the Adams type. We thus conclude that both staggered-Wilson fermions have proper charge conjugation symmetry.

TABLE I: Symmetries of staggered-Wilson fermions.

	N_f	$\mathcal{S}$&$\mathcal{I}$-subgroup	$\mathcal{R}$-subgroup	P	C	SW_4
Staggered	4	$\mathcal{S}_\mu,\ \mathcal{I}_\mu$	$\mathcal{R}_{\mu\nu}$	◯	◯	◯
Adams	2	$\mathcal{S}_\mu\mathcal{S}_\nu,\ \mathcal{S}_\mu\mathcal{I}_\mu$	$\mathcal{R}_{\mu\nu}$	◯	◯	◯
Hoelbling	1	$\mathcal{S}_\mu\mathcal{S}_\nu\mathcal{S}_\rho\mathcal{S}_\sigma,\ \mathcal{S}_\mu\mathcal{I}_\mu$	$\mathcal{R}_{\mu\nu}\mathcal{R}_{\rho\sigma}$	◯	◯	×

We lastly consider hypercubic symmetry. In staggered fermions, the rotation Eq. (15) and axis reversal Eq. (14) form hypercubic symmetry [27], which enhances to Euclidian Lorentz symmetry in the continuum limit. In the case of the Adams-type fermion, the action is invariant under the rotation Eq. (15) and the shifted-axis reversal $\mathcal{S}_\mu\mathcal{I}_\mu$. These two symmetries can form proper hypercubic symmetry SW_4 in this case. Thus we conclude that Adams fermion recovers Lorentz symmetry in the continuum. In the Hoelbling-type formulation, the action breaks the rotation symmetry into its subgroup called doubled rotation [10], which is given by

$$\mathcal{R}_{\rho\sigma}\mathcal{R}_{\mu\nu} \sim \exp[\frac{\pi}{4}(\Gamma_\rho\Gamma_\sigma + \Gamma_\mu\Gamma_\nu)]\exp[\frac{\pi}{4}(\Xi_\rho\Xi_\sigma + \Xi_\mu\Xi_\nu)]\phi(R_{\rho\sigma}^{-1}R_{\mu\nu}^{-1}p) \ , \tag{22}$$

where (μ,ν,σ,ρ) is any permutation of $(1,2,3,4)$. It is also invariant under sequential transformations of (μ,ν rotation), (ν,μ rotation), (μ shift) and (ν shift) as

$$\mathcal{S}_\nu\mathcal{S}_\mu\mathcal{R}_{\nu\mu}\mathcal{R}_{\mu\nu} \sim \exp(ip_\mu + ip_\nu)\Gamma_\mu\Gamma_\nu\,\phi(\tilde{p}) \ , \tag{23}$$

with $\tilde{p}_{\mu,\nu} = -p_{\mu,\nu}, \tilde{p}_\tau = p_\tau,\ \tau \neq \mu,\nu$. The loss of rotation symmetry indicates that we cannot define hypercubic symmetry in the Hoelbling fermion. It implies that it could not

lead to a correct continuum theory, and we would need to tune parameters to restore Lorentz symmetry. Indeed the recent study on symmetries of staggered-Wilson fermions by Sharpe [28] reports that recovery of Lorentz symmetry requires fine-tuning of coefficients in the gluonic sector in lattice QCD with Hoelbling fermion.

To summarize, Adams fermion possesses physical parity, charge conjugation and hypercubic symmetries while Hoelbling fermion loses hypercubic as shown in Table. I. It seems that Hoelbling fermion cannot be straightforwardly applied to lattice QCD while Adams type can. We note that both staggered-Wilson fermions have proper parity symmetry, and we can discuss spontaneous parity symmetry breaking. Moreover, we may find some symptom due to Lorentz symmetry breaking in Hoelbling fermion in the parity-phase structure. This is another motivation to study parity-phase structure in strong-coupling lattice QCD.

In the end of this section, we comment on special symmetries in staggered-Wilson fermions without mass shift. Hoelbling fermion without the mass shift $(\eta_\mu D_\mu + M_H)$ possesses special charge conjugation symmetry $(\mathcal{C}'_T : \chi \to \bar{\chi},\ \bar{\chi} \to \chi)$. This topic is beyond the scope of this work, but we note that it can do good to two flavors in the central branch. Use of the central branch is intensively discussed in [11, 29].

IV. HOPPING PARAMETER EXPANSION

In this section we investigate parity-phase structure in lattice QCD with staggered-Wilson fermions in the framework of hopping parameter expansion (HPE) in the strong-coupling regime [12]. In the hopping parameter expansion, we treat a mass term as a leading action while we perturbatively treat hopping terms. We thus perform expansion by a hopping parameter which essentially corresponds to inverse of a mass parameter. By using self-consistent equations we derive one- and two-point functions, and calculate meson condensates and meson mass for two types of staggered-Wilson fermions. We for simplicity drop the flavor indices until we discuss the two-flavor case in details in Sec. VI. However it is easy to recover the flavor indices for the field χ_f, the mass parameter M_f and the condensate Σ_f $(f = 1, 2, ...)$.

$0-$ hopping (mass term)

(x,a) ●—— (y,b) $\qquad \langle \chi^a_x \bar{\chi}^b_y \rangle_0 = -\delta_{xy}\delta^{ab}$

$1-$ hopping (kinetic term)

$(x,a) \longrightarrow (x+\hat{\mu},b)$ $\qquad K\eta_{\mu,x}(U_{\mu,x})^{ab}$

$(x,b) \longleftarrow (x+\hat{\mu},a)$ $\qquad -K\eta_{\mu,x}(U^\dagger_{\mu,x})^{ab}$

$2-$ hopping (flavored mass term)

$(x,a) \longrightarrow x+\alpha\hat{\mu} \longrightarrow (x+\alpha\hat{\mu}+\beta\hat{\nu},b)$ $\qquad 2Kri\eta_{\mu\nu,x}(\mathcal{W}^{(2)}_{\alpha\mu\beta\nu,x})^{ab}/(2^3\sqrt{3})$

$(x,b) \longleftarrow x+\alpha\hat{\mu} \longleftarrow (x+\alpha\hat{\mu}+\beta\hat{\nu},a)$ $\qquad -2Kri\eta_{\mu\nu,x}(\mathcal{W}^{(2)\dagger}_{\alpha\mu\beta\nu,x})^{ab}/(2^3\sqrt{3})$

FIG. 1: Feynman rules in hopping parameter expansion (HPE) with the Hoelbling-type staggered-Wilson fermion. a and b stand for the color indices. $\mathcal{W}^{(2)}_{\alpha\mu\beta\nu,x}$ is given in Table II.

TABLE II: Concrete forms of $\mathcal{W}^{(2)}_{\alpha\mu\beta\nu,x}$ in Fig. 1.

α	β	$\mathcal{W}^{(2)}_{\alpha\mu\beta\nu,x}$
$+$	$+$	$U_{\mu,x}U_{\nu,x+\hat{\mu}}$
$-$	$-$	$U^\dagger_{\mu,x-\hat{\mu}}U^\dagger_{\nu,x-\hat{\mu}-\hat{\nu}}$
$+$	$-$	$U_{\mu,x}U^\dagger_{\nu,x+\hat{\mu}-\hat{\nu}}$
$-$	$+$	$U^\dagger_{\mu,x-\hat{\mu}}U_{\nu,x-\hat{\mu}}$

A. Hoelbling type

We begin with the Hoelbling-type fermion, which contains two-hopping terms in the action. One reason that we start with Hoelbling type regardless of the lower rotation symmetry is that 2-hopping calculation can be a good exercise for 4-hopping case in Adams type. To perform the HPE for the Hoelbling-type fermion, we rewrite the action Eq. (12) by redefining $\chi \to \sqrt{2K}\chi$ with the hopping parameter $K = 1/[2(M+2r)]$,

$$S = \sum_x \bar{\chi}_x\chi_x + 2K\sum_{x,y}\bar{\chi}_x(\eta_\mu D_\mu)_{xy}\chi_y + 2Kr\sum_{x,y}\bar{\chi}_x(M_H)_{xy}\chi_y \ , \tag{24}$$

where M_H is given by Eq. (6). The plaquette action is $1/g^2$ term and we can omit it in the strong-coupling limit. In this section, we derive one- and two-point functions by using a $\mathcal{O}(K^3)$ self-consistent equation: Solving this equation leads to truncation of diagrams as the

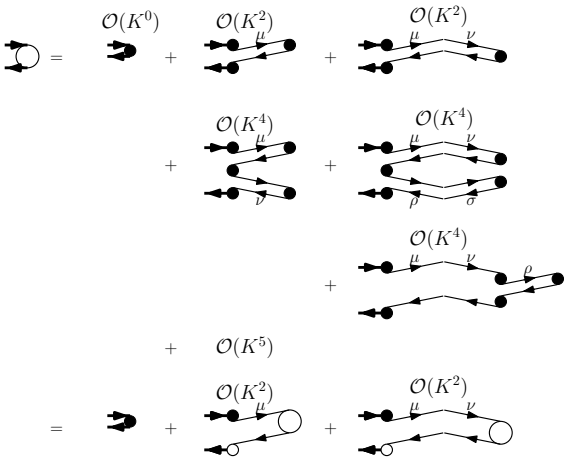

FIG. 2: Feynman diagram for mesonic one-point functions in the $\mathcal{O}(K^3)$ self-consistent equation of HPE with the Hoelbling fermion. Black circles stand for the leading one-point function $\langle \chi_x \bar{\chi}_x \rangle_0$ while white circles stand for $\langle \chi_x \bar{\chi}_x \rangle$ which include next-leading and higher hopping terms. By summing up higher contributions, we obtain the second equality.

ladder approximation having all diagrams to $\mathcal{O}(K^3)$ are taken into account. More precisely, this approximation does not take account of all diagrams, but it successfully includes certain kinds of diagrams to all orders of K thanks to a self-consistent approach. We thus expect that it works to figure out existence of Aoki phase. We note that this approximation especially works well for a small hopping parameter $K \ll 1$. In Fig. 1, we depict Feynman rules in the HPE for this fermion. The fundamental Feynman rules contain contributions from 0-hopping (mass term), 1-hopping (kinetic term) and 2-hopping (flavored-mass term) terms.

First, by using these Feynman rules, we derive meson condensates from an one-point function of the meson operator $\mathcal{M}_x = \bar{\chi}_x \chi_x$ in the mean-field approximation. The one-point function is defined as

$$\langle \chi_x^a \bar{\chi}_x^b \rangle \equiv -\delta_{ab} \Sigma_x = \frac{\int \mathcal{D}[\chi, \bar{\chi}, U] \chi_x^a \bar{\chi}_x^b \; e^S}{\int \mathcal{D}[\chi, \bar{\chi}, U] e^S} \; . \tag{25}$$

Note that we use the partition function $Z = \int \mathcal{D}[\chi, \bar{\chi}, U] e^S$, not $Z = \int \mathcal{D}[\chi, \bar{\chi}, U] e^{-S}$, following the convention for the partition function in the strong-coupling analysis [24]. The leading term in the hopping parameter expansion is given by

$$\langle \chi_x^a \bar{\chi}_x^b \rangle_0 = \frac{\int \mathcal{D}[\chi, \bar{\chi}, U] \, \chi_x^a \bar{\chi}_x^b \; e^{S_0}}{\int \mathcal{D}[\chi, \bar{\chi}, U] \, e^{S_0}} = -\delta^{ab} \; , \tag{26}$$

where $S_0 = \sum_x \bar{\chi}_x \chi_x$. By using the Feynman rules, we can evaluate the diagrams in Fig. 2.

$$
\begin{aligned}
\langle \chi^a_x \bar{\chi}^b_x \rangle &\equiv -\delta^{ab}\Sigma_x \\
&= \langle \chi^a_x \bar{\chi}^b_x \rangle_0 \\
&+ \sum_{\pm\mu} (-1)(K\eta_{\mu,x})^2 \langle (\chi^a \bar{\chi})_x \rangle_0 U_{\mu,x} \langle (\chi\bar{\chi})_{x+\hat{\mu}} \rangle_0 U^\dagger_{\mu,x} \langle (\chi \bar{\chi}^b)_x \rangle_0 \\
&+ \sum_{\substack{\pm\mu,\pm\nu \\ (\mu\neq\nu)}} (-1) \left(2Kri\eta_{\mu\nu,x} \frac{1}{2^3\sqrt{3}} \right)^2 \langle (\chi^a \bar{\chi})_x \rangle_0 \mathcal{W}^{(2)}_{\mu\nu,x} \langle (\chi\bar{\chi})_{x+\hat{\mu}+\hat{\nu}} \rangle_0 \mathcal{W}^{(2)\dagger}_{\mu\nu,x} \langle (\chi \bar{\chi}^b)_x \rangle_0 \\
&+ \sum_{\pm\mu,\pm\nu} (-1)(K\eta_{\mu,x})^2 (-1)(K\eta_{\nu,x})^2 \langle (\chi^a \bar{\chi})_x \rangle_0 U_{\mu,x} \langle (\chi\bar{\chi})_{x+\hat{\mu}} \rangle_0 U^\dagger_{\mu,x} \langle (\chi\bar{\chi})_x \rangle_0 U_{\nu,x} \\
&\times \langle (\chi\bar{\chi})_{x+\hat{\nu}} \rangle_0 U^\dagger_{\nu,x} \langle (\chi \bar{\chi}^b)_x \rangle_0 \\
&+ \sum_{\substack{\pm\mu,\pm\nu,\pm\rho,\pm\sigma \\ (\mu\neq\nu,\rho\neq\sigma)}} (-1) \left(2Kri\eta_{\mu\nu,x} \frac{1}{2^3\sqrt{3}} \right)^2 (-1) \left(2Kri\eta_{\rho\sigma,x} \frac{1}{2^3\sqrt{3}} \right)^2 \\
&\times \langle (\chi^a \bar{\chi})_x \rangle_0 \mathcal{W}^{(2)}_{\mu\nu,x} \langle (\chi\bar{\chi})_{x+\hat{\mu}+\hat{\nu}} \rangle_0 \mathcal{W}^{(2)\dagger}_{\mu\nu,x} \langle (\chi\bar{\chi})_x \rangle_0 \mathcal{W}^{(2)}_{\rho\sigma,x} \langle (\chi\bar{\chi})_{x+\hat{\rho}+\hat{\sigma}} \rangle_0 \mathcal{W}^{(2)\dagger}_{\rho\sigma,x} \langle (\chi \bar{\chi}^b)_x \rangle_0 \\
&+ \sum_{\substack{\pm\mu,\pm\nu,\pm\rho \\ (\mu\neq\nu)}} (-1) \left(2Kri\eta_{\mu\nu,x} \frac{1}{2^3\sqrt{3}} \right)^2 (-1) \left(K\eta_{\rho,x} \right)^2 \langle (\chi^a \bar{\chi})_x \rangle_0 \mathcal{W}^{(2)}_{\mu\nu,x} \\
&\times \langle (\chi\bar{\chi})_{x+\hat{\mu}+\hat{\nu}} \rangle_0 U_{\rho,x+\hat{\mu}+\hat{\nu}} \langle (\chi\bar{\chi})_{x+\hat{\mu}+\hat{\nu}+\hat{\rho}} \rangle_0 U^\dagger_{\rho,x+\hat{\mu}+\hat{\nu}} \langle (\chi\bar{\chi})_{x+\hat{\mu}+\hat{\nu}} \rangle_0 \mathcal{W}^{(2)\dagger}_{\mu\nu,x} \langle (\chi \bar{\chi}^b)_x \rangle_0 \\
&+ \mathcal{O}(K^5) \ , \qquad (27)
\end{aligned}
$$

where $(\chi\bar{\chi})_x$ stands for $\chi_x\bar{\chi}_x$ and $\mathcal{W}^{(2)}_{\mu\nu,x} = \mathcal{W}^{(2)}_{+\mu+\nu,x}$ in Table. II. Note that we consider only connected diagrams in Fig. 2. By summing higher hopping terms, the one-point function is obtained as shown in Fig. 2, which is given by

$$
-\Sigma_x \equiv -\langle \mathcal{M}_x \rangle = -\langle \mathcal{M}_x \rangle_0 + 2K^2 \sum_\mu \Sigma_x \Sigma_{x+\hat{\mu}} - 2 \cdot \frac{1}{24} (Kr)^2 \sum_{\mu\neq\nu} \Sigma_x \Sigma_{x+\hat{\mu}+\hat{\nu}} \ . \qquad (28)
$$

The equation contains terms to $\mathcal{O}(K^2)$, and $\mathcal{O}(K^3)$ diagrams are found to vanish due to cancellation between the diagrams. Here we solve it in a self-consistent way for condensate Σ within mean-field approximation. We here assume $\Sigma_x = \sigma_x + i\epsilon_x\pi_x$ as the condensate. σ and π correspond to chiral and pion condensates, respectively. We substitute this form of Σ_x in Eq. (28) and obtain a self-consistent equation

$$
-(\sigma + i\epsilon_x\pi) = -1 + 2K^2 \cdot 4 \left(\sigma^2 + \pi^2 \right) - 2 \cdot \frac{1}{24} (Kr)^2 \cdot 4 \cdot 3 \left(\sigma + i\epsilon_x\pi \right)^2 \ , \qquad (29)
$$

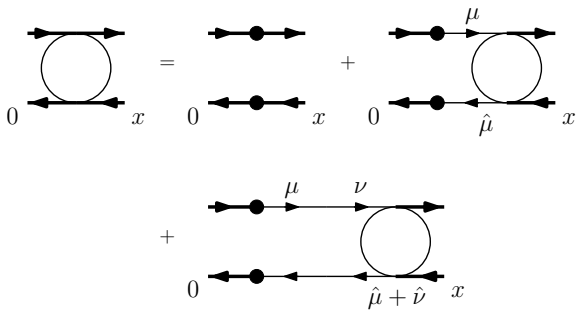

FIG. 3: Feynman diagram for mesonic two-point functions for $\mathcal{O}(K^3)$ self-consistent equation with the Hoelbling fermion.

which yields $-\sigma = -1 + 16K^2\pi^2$ and $-i\pi = -8K^2 \cdot 2i\sigma\pi$. For simplicity, we have set $r = 2\sqrt{2}$ to make the equation Eq. (29) simpler. Of course we can also discuss for other values of r in general.

Now we have two solutions depending on $\pi = 0$ or $\pi \neq 0$: For $\pi = 0$, we have a trivial solution $\sigma = 1$. For $\pi \neq 0$, we have a solution as

$$\sigma = \frac{1}{16K^2}, \qquad \pi = \pm\sqrt{\frac{1}{16K^2}\left(1 - \frac{1}{16K^2}\right)}\ . \tag{30}$$

Nonzero pion condensate implies spontaneous parity breaking for the range $\mid K \mid > 1/4$. The sign of the pion condensate in Eq. (30) reflects the Z_2 parity symmetry of the theory. Thus the parity-broken phase, if it exists, appears in a parameter range $-4\sqrt{2}-2 < M < -4\sqrt{2}+2$ in the strong-coupling limit. We note that the critical hopping parameter $|K_c| = 1/4$ is small, and we speculate that the $\mathcal{O}(K^3)$ self-consistent equation is valid around the value.

Next, we discuss the meson mass from a two-point function of the meson operator $\mathcal{S}(0,x) \equiv \langle \mathcal{M}_0 \mathcal{M}_x \rangle$. From Fig. 3, we derive the following $\mathcal{O}(K^3)$ equation for a two-point function.

$$\begin{aligned}
\mathcal{S}(0,x) =& \langle \bar{\chi}_0^a \chi_0^a \bar{\chi}_x^b \chi_x^b \rangle \\
=& -\delta_{0x} N_c \\
& - K^2 \langle \bar{\chi}_0^a \chi_0^a \bar{\chi}_0^c (\eta_{\mu,0})^2 \left[U_{\mu,0}^{cd} \chi_{\hat{\mu}}^d \bar{\chi}_{\hat{\mu}}^e (U_{\mu,0}^\dagger)^{ef} + (U_{\mu,-\hat{\mu}}^\dagger)^{cd} \chi_{-\hat{\mu}}^d \bar{\chi}_{-\hat{\mu}}^e U_{\mu,-\hat{\mu}}^{ef} \right] \chi_0^f \bar{\chi}_x^b \chi_x^b \rangle \\
& - \left(2Kri \frac{1}{2^3\sqrt{3}} \right)^2 \langle \bar{\chi}_0^a \chi_0^a \bar{\chi}_0^c \sum_{\alpha,\beta=\pm} \sum_{\mu \neq \nu} (\eta_{\mu\nu,0})^2 \left[(\mathcal{W}^{(2)}_{\alpha\mu\beta\nu,0})^{cd} \chi^d_{\alpha\hat{\mu}\beta\hat{\nu}} \bar{\chi}^e_{\alpha\hat{\mu}\beta\hat{\nu}} (\mathcal{W}^{(2)\dagger}_{\alpha\mu\beta\nu,0})^{ef} \right] \chi_0^f \bar{\chi}_x^b \chi_x^b \rangle\ ,
\end{aligned} \tag{31}$$

where $\mathcal{W}^{(2)}_{\alpha\mu\beta\nu,0}$ is defined in Table. II. Note that we consider only connected diagrams in Fig. 3. By integrating out the link variables in the strong-coupling limit, it is simplified as

$$\mathcal{S}(0,x) \equiv \langle \bar{\chi}^a_0 \chi^a_0 \bar{\chi}^b_x \chi^b_x \rangle = -\delta_{0x} N_c + K^2 \sum_{\pm\mu} \langle \chi^a_{\hat{\mu}} \bar{\chi}^a_{\hat{\mu}} \bar{\chi}^b_x \chi^b_x \rangle + \left(2Kri \frac{1}{2^3\sqrt{3}} \right)^2 \sum_{\substack{\pm\mu,\pm\nu \\ (\mu\neq\nu)}} \langle \chi^a_{\hat{\mu}+\hat{\nu}} \bar{\chi}^a_{\hat{\mu}+\hat{\nu}} \bar{\chi}^b_x \chi^b_x \rangle \ . \tag{32}$$

Then the self-consistent equation for $\mathcal{S}$ is given in the momentum space as

$$\mathcal{S}(p) = -N_c + \Bigg[-K^2 \sum_\mu \left(e^{-ip_\mu} + e^{ip_\mu} \right) + \left(2Kr \frac{1}{2^3\sqrt{3}} \right)^2 \sum_{\mu\neq\nu} \left(e^{-i(p_\mu+p_\nu)} + e^{i(p_\mu+p_\nu)} + e^{-i(p_\mu-p_\nu)} + e^{i(p_\mu-p_\nu)} \right) \Bigg] \mathcal{S}(p) \ . \tag{33}$$

We finally obtain the meson propagator as

$$\mathcal{S}(p) = N_c \left[-2K^2 \sum_\mu \cos p_\mu + 4 \left(2Kr \frac{1}{2^3\sqrt{3}} \right)^2 \sum_{\mu\neq\nu} \cos p_\mu \cos p_\nu - 1 \right]^{-1} \ . \tag{34}$$

Here the pole of $\mathcal{S}(p)$ should give meson mass. Since χ is an one-component fermion, it may seem to be difficult to find the pion excitation from Eq. (34). However, as we discussed, γ_5 in the staggered fermion is given by $\epsilon_x = (-1)^{x_1+\ldots+x_4}$ and the pion operator is given by $\pi_x = \bar{\chi}_x i\epsilon_x \chi_x$. We therefore identify momentum of pion by measuring it from a shifted origin $p = (\pi, \pi, \pi, \pi)$. Here we set $p = (im_\pi a + \pi, \pi, \pi, \pi)$ for $1/\mathcal{S}(p) = 0$ in Eq. (34). Then we derive the pion mass m_π as

$$\cosh(m_\pi a) = 1 + \frac{1 - 16K^2}{6K^2} \ , \tag{35}$$

where we again set $r = 2\sqrt{2}$ for simplicity. In this result, the pion mass becomes zero at $|K| = 1/4$, and tachyonic in the range $\mid K \mid > 1/4$. It implies that there occurs a phase transition between parity-symmetric and parity-broken phases at $|K| = 1/4$, which is consistent with the result from the one-point function in Eq. (30). We note that the massless pion at the phase boundary is consistent with the scenario of second-order transition. We can also derive the sigma meson mass by substituting $p = (im_\pi a, 0, 0, 0)$ for $1/\mathcal{S}(p) = 0$ in Eq. (34) as

$$\cosh(m_\sigma a) = 1 + \frac{1}{2K^2} \ . \tag{36}$$

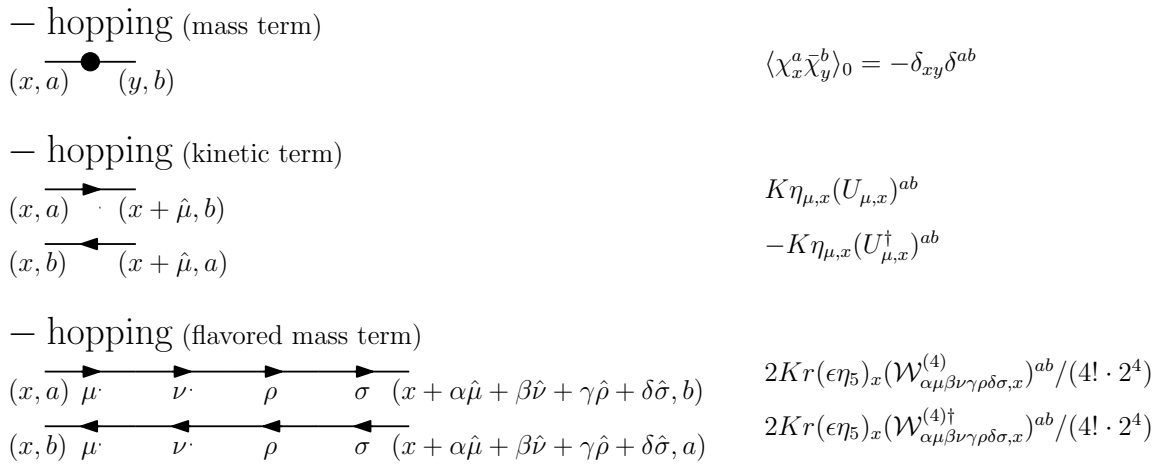

FIG. 4: Feynman rules for the HPE with the Adams fermion. a and b stand for the color indices. We show the concrete forms of $\mathcal{W}^{(4)}_{\alpha\mu\beta\nu\gamma\rho\delta\sigma,x}$ in Table III of Appendix B.

B. Adams type

We investigate the parity-phase structure for the Adams-type staggered-fermion by using $\mathcal{O}(K^3)$ self-consistent equations in hopping parameter expansion. The approach is basically parallel to that of Hoelbling type. We just need to consider Feynman diagrams for this case. The action Eq. (10) is rewritten by redefining $\chi \to \sqrt{2K}\chi$ with $K = 1/[2(M+r)]$ as,

$$S = \sum_x \bar{\chi}_x \chi_x + 2K \sum_{x,y} \bar{\chi}_x (\eta_\mu D_\mu)_{xy} \chi_y + 2Kr \sum_{x,y} \bar{\chi}_x (M_A)_{xy} \chi_y \ , \tag{37}$$

where M_A is given in Eq. (1). In Fig. 4, the Feynman rules in the HPE for this fermion are depicted. First, we derive meson condensates from the one-point function $\mathcal{M}_x = \bar{\chi}_x \chi_x$. The equation for the one-point function is obtained as shown in Fig. 5,

$$\begin{aligned} -\Sigma_x &\equiv -\langle \mathcal{M}_x \rangle \\ &= -\langle \mathcal{M}_x \rangle_0 + 2K^2 \sum_\mu \Sigma_x \Sigma_{x+\hat{\mu}} - 2 \cdot \frac{1}{(4!)^2 \cdot 2^3} (Kr)^2 \sum_{\mu \neq \nu \neq \rho \neq \sigma} \Sigma_x \Sigma_{x+\hat{\mu}+\hat{\nu}+\hat{\rho}+\hat{\sigma}} \ . \end{aligned} \tag{38}$$

We substitute $\Sigma_x = \sigma_x + i\epsilon_x \pi_x$ for Σ_x in Eq. (38) and obtain the self-consistent equation

$$-(\sigma + i\epsilon_x \pi) = -1 + 2K^2 \cdot 4 \left(\sigma^2 + \pi^2\right) - 2 \cdot \frac{1}{(4!)^2 \cdot 2^3} (Kr)^2 \cdot 4! \left(\sigma + i\epsilon_x \pi\right)^2 \ . \tag{39}$$

From this, we obtain $-\sigma = -1 + 16K^2\pi^2$ and $-i\pi = -8K^2 \cdot 2i\sigma\pi$. Here we have set $r = 16\sqrt{3}$ to make the equation simple. We again have two solutions: For $\pi = 0$, we have a trivial

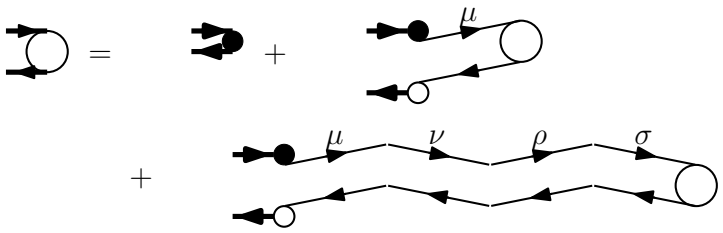

FIG. 5: Feynman diagram for mesonic one-point functions in the $\mathcal{O}(K^3)$ self-consistent equations of HPE with the Adams fermion. There is a 4-hopping fundamental diagram, which is peculiar to this fermion.

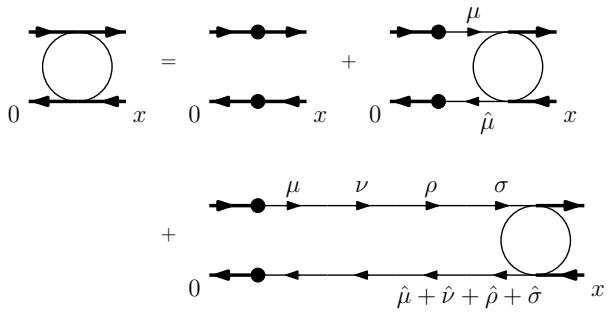

FIG. 6: Feynman diagram for mesonic two-point functions for $\mathcal{O}(K^3)$ self-consistent equations of HPE with the Adams fermion.

solution $\sigma = 1$. For $\pi \neq 0$, we have a non-trivial solution as

$$\sigma = \frac{1}{16K^2}, \qquad \pi = \pm\sqrt{\frac{1}{16K^2}\left(1 - \frac{1}{16K^2}\right)}\ . \tag{40}$$

It indicates that parity-broken phase appears in the range of the hopping parameter as $\mid K \mid > 1/4$ or equivalently $-16\sqrt{3} - 2 < M < -16\sqrt{3} + 2$.

Next, we discuss the meson mass from a two-point function of the meson operator $\mathcal{S}(0, x) \equiv \langle \mathcal{M}_0 \mathcal{M}_x \rangle$. From Fig. 6 we derive the following equation for two-point functions,

$$
\begin{aligned}
\mathcal{S}(0,x) =& \langle \bar{\chi}_0^a \chi_0^a \bar{\chi}_x^b \chi_x^b \rangle \\
=& -\delta_{0x} N_c \\
& - K^2 \langle \bar{\chi}_0^a \chi_0^a \bar{\chi}_0^c (\eta_{\mu,0})^2 \Big[U_{\mu,0}^{cd} \chi_{\hat{\mu}}^d \bar{\chi}_{\hat{\mu}}^e (U_{\mu,0}^\dagger)^{ef} + (U_{\mu,-\hat{\mu}}^\dagger)^{cd} \chi_{-\hat{\mu}}^d \bar{\chi}_{-\hat{\mu}}^e U_{\mu,-\hat{\mu}}^{ef} \Big] \chi_0^f \bar{\chi}_x^b \chi_x^b \rangle \\
& + \left(2Kr\epsilon\eta_5 \frac{1}{4! \cdot 2^4} \right)^2 \langle \bar{\chi}_0^a \chi_0^a \bar{\chi}_0^c \sum_{\alpha,\beta,\gamma,\delta=\pm} \sum_{\mu\neq\nu\neq\rho\neq\sigma} \Big[\left(\mathcal{W}^{(4)}_{\alpha\mu\beta\nu\gamma\rho\delta\sigma,0} \right)^{cd} \chi^d_{\alpha\hat{\mu}\beta\hat{\nu}\gamma\hat{\rho}\delta\hat{\sigma}} \bar{\chi}^e_{\alpha\hat{\mu}\beta\hat{\nu}\gamma\hat{\rho}\delta\hat{\sigma}} \\
& \times \left(\mathcal{W}^{(4)\dagger}_{\alpha\mu\beta\nu\gamma\rho\delta\sigma,0} \right)^{ef} \Big] \chi_0^f \bar{\chi}_x^b \chi_x^b \rangle \ , \qquad (41)
\end{aligned}
$$

where $\mathcal{W}^{(4)}_{\alpha\mu\beta\nu\gamma\rho\delta\sigma,x}$ is defined in Table. III of Appendix B. By integrating out the link variables in the strong-coupling limit, it is simplified as

$$
\begin{aligned}
\mathcal{S}(0,x) \equiv \langle \bar{\chi}_0^a \chi_0^a \bar{\chi}_x^b \chi_x^b \rangle =& -\delta_{0x} N_c + K^2 \sum_{\pm\mu} \langle \chi_{\hat{\mu}}^a \bar{\chi}_{\hat{\mu}}^a \bar{\chi}_x^b \chi_x^b \rangle \\
& - \left(2Kr \frac{1}{4! \cdot 2^4} \right)^2 \sum_{\substack{\pm\mu,\pm\nu,\pm\rho,\pm\sigma \\ (\mu\neq\nu\neq\rho\neq\sigma)}} \langle \chi^a_{\hat{\mu}+\hat{\nu}+\hat{\rho}+\hat{\sigma}} \bar{\chi}^a_{\hat{\mu}+\hat{\nu}+\hat{\rho}+\hat{\sigma}} \bar{\chi}_x^b \chi_x^b \rangle \ . \qquad (42)
\end{aligned}
$$

Then the self-consistent equation for $\mathcal{S}$ is given in the momentum space as

$$
\begin{aligned}
\mathcal{S}(p) = -N_c + \Bigg[& -K^2 \sum_\mu \left(e^{-ip_\mu} + e^{ip_\mu} \right) \\
& + \left(2Kr \frac{1}{4! \cdot 2^4} \right)^2 \sum_{\alpha,\beta,\gamma,\delta=\pm} \sum_{\mu\neq\nu\neq\rho\neq\sigma} e^{+i(\alpha p_\mu + \beta p_\nu + \gamma p_\rho + \delta p_\sigma)} \Bigg] \ . \qquad (43)
\end{aligned}
$$

We finally obtain the meson propagator as

$$
S(p) = N_c \Bigg[-2K^2 \sum_\mu \cos p_\mu + 16 \left(2Kr \frac{1}{4! \cdot 2^4} \right)^2 \sum_{\mu\neq\nu\neq\rho\neq\sigma} \cos p_\mu \cos p_\nu \cos p_\rho \cos p_\sigma - 1 \Bigg]^{-1} \ . \qquad (44)
$$

Here we set $p = (im_\pi a + \pi, \pi, \pi, \pi)$ for $1/\mathcal{S}(p) = 0$ in Eq. (44), which gives the pion mass m_π as

$$
\cosh(m_\pi a) = 1 + \frac{1 - 16K^2}{10K^2} \ , \qquad (45)
$$

where we again set $r = 16\sqrt{3}$ for simplicity. Here the pion mass becomes zero at $\mid K \mid = 1/4$ and becomes tachyonic in the range $\mid K \mid > 1/4$. It suggests that there occurs a second-order phase transition between parity-symmetric and broken phases at $|K| = 1/4$, which is consistent with Eq. (40). We can also derive the sigma meson mass by substituting $p = (im_\pi a, 0, 0, 0)$ for $1/\mathcal{S}(p) = 0$ in Eq. (44) as

$$
\cosh(m_\sigma a) = 1 + \frac{1}{6K^2} \ . \qquad (46)
$$

V. EFFECTIVE POTENTIAL ANALYSIS

In the previous section, we have investigated the parity-phase structure in hopping parameter expansion. We found a strong sign of parity-broken phase for $\mid K \mid > 1/4$. In order to judge whether the parity-broken phase is realized as a vacuum, the analysis of the gap solution in the hopping parameter expansion is not enough, and we need to investigate the effective potential for meson fields.

In this section, we consider the effective potential of meson fields for $SU(N)$ lattice gauge theory with staggered-Wilson fermions. In the strong-coupling limit and the large N limit, effective action can be exactly derived by integrating the link variables [12, 24]. Then, by solving a saddle-point equation, we can investigate a vacuum and find meson condensations. In this section we again begin with the Hoelbling case as exercise, and go on to Adams fermion with better discrete symmetry.

A. Hoelbling type

In the strong-coupling limit we can drop plaquette action. Then the partition function for meson fields $\mathcal{M}_x = (\bar{\chi}_x \chi_x)/N$ with the source J_x is given by

$$Z(J) = \int \mathcal{D}\left[\chi, \bar{\chi}, U\right] \exp\left[N \sum_x J_x \mathcal{M}_x + S_F \right] \ . \tag{47}$$

where S_F stands for the fermion action. Here we have defined $\mathcal{M}_x$ with a $1/N$ factor to ensure it to have a certain large N limit. In this case, S_F is the Hoelbling-type staggered-Wilson action Eq. (12). N stands for the number of color. In the large N limit, we can perform the link integral. We here consider the effective action up to $\mathcal{O}(\mathcal{M}^3)$ for meson field $\mathcal{M}$. This order corresponds to the $\mathcal{O}(K^3)$ self-consistent equation in the hopping parameter expansion.

We develop a method to perform the link-variable integral with multi-hopping fermion action terms. In our method, we perform the link integral by introducing two kinds of link-variable measures. Now we formally rewrite the partition function as,

$$Z(J) = \int \mathcal{D}\left[\chi, \bar{\chi}\right] \exp\left[\sum_x N \left(J_x + \hat{M} \right) \mathcal{M}_x \right] \exp\left[\sum_x N W(\Lambda) \right] \ , \tag{48}$$

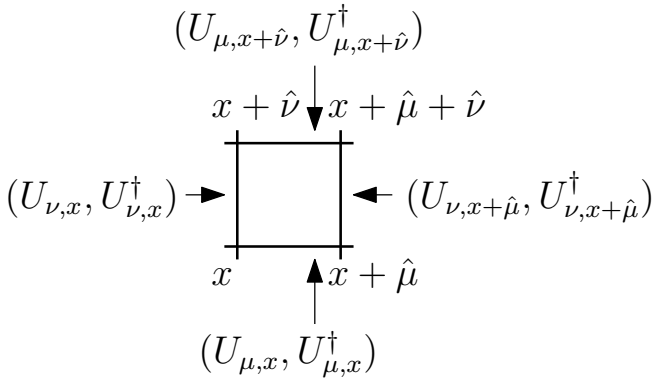

FIG. 7: Link variables corresponding to the two kinds of measures in the partition function Eq. (49) in a 2 dimensional case.

where we define $\hat{M} = M + 2r$ and the last term is expressed as,

$$\exp\left[\sum_x NW(\Lambda)\right] = \prod_x Z_x \ ,$$
$$Z_x = \int \left(\prod_{\mu\neq\nu} \mathcal{D}\left[U_{\mu,x}, U_{\mu,x+\hat{\nu}}\right]\right) \exp\left[-\left(\mathrm{Tr}(VE^\dagger) - \mathrm{Tr}(V^\dagger E)\right)\right] \ . \qquad (49)$$

Λ, E and $E^\dagger$ (V and $V^\dagger$) are composites of the fermion field χ (link variables U), which we will explicitly show later. $W(\Lambda)$ is a function of Λ, which will be an essential part of effective potential of meson fields.

Now we explain how the integral in Eq. (49) can be performed by using two types of the link measure. Let us consider two-dimensional cases in Fig. 7 for simplicity. In this case, $U_{\mu,x}$ and $U_{\mu,x+\hat{\nu}}$ ($\mu \neq \nu$) form link variables in a square block. We can classify diagrams to $\mathcal{O}(\mathcal{M}^3)$ into three types: (1) 1-link (μ) + 1-link ($-\mu$) hoppings, (2) 2-link (μ, ν) + 2-link ($-\nu, -\mu$) hoppings, (3) 2-link (μ, ν) + 1-link ($-\nu$) + 1-link ($-\mu$) hoppings. The 1-link hopping comes from the usual staggered kinetic term while the 2-link hopping from the flavored-mass term. (1) and (2) are $\mathcal{O}(\mathcal{M}^2)$ while (3) is $\mathcal{O}(\mathcal{M}^3)$. Since one square block contains all the three diagrams, we can derive the effective potential by integrating link variables per each block. We note that $\mathcal{O}(\mathcal{M}^3)$ diagrams cancel between one another, which is consistent with the HPE calculations. We can also avoid double-counting by adjusting factors for one-link and two-link terms as we will show in Eq. (64).

In this method, we need to define sets of link variables and fermion bilinears as V and E in Eq. (49) : V and E are matrices including components corresponding to 1- and 2-link

terms. We call a space spanned by these matrices "hopping space". Here we define a, b and α, β as color and hopping space indices respectively. We also denote Tr as trace for color and the hopping space. Explicit forms of V and E are given by

$$V^{ab}_{\alpha\beta} = \mathrm{diag}\left(V^{ab}_1, V^{ab}_2, V^{ab}_3\right) \ , \tag{50}$$

with

$$\begin{aligned} V_1 &= \mathrm{diag}\left(U_{\mu,x}\right) \\ &\equiv \mathrm{diag}\underbrace{\left(U_{1,x}, U_{2,x}, \cdots, U_{4,x}\right)}_{4} \ , \end{aligned} \tag{51}$$

$$\begin{aligned} V_2 &= \mathrm{diag}\left(U_{\mu,x}U_{\nu,x+\hat{\mu}}\right) \\ &\equiv \mathrm{diag}\underbrace{\left(U_{1,x}U_{2,x+\hat{1}}, U_{1,x}U_{3,x+\hat{1}}, \cdots, U_{4,x}U_{3,x+\hat{4}}\right)}_{12} \ , \end{aligned} \tag{52}$$

$$\begin{aligned} V_3 &= \mathrm{diag}\left(U_{\mu,x+\hat{\nu}}U^\dagger_{\nu,x+\hat{\mu}}\right) \\ &\equiv \mathrm{diag}\underbrace{\left(U_{1,x+\hat{2}}U^\dagger_{2,x+\hat{1}}, U_{1,x+\hat{3}}U^\dagger_{3,x+\hat{1}}, \cdots, U_{4,x+\hat{3}}U^\dagger_{3,x+\hat{4}}\right)}_{12} \ , \end{aligned} \tag{53}$$

$$E^{ab}_{\alpha\beta} = \mathrm{diag}\left(E^{ab}_1, E^{ab}_2, E^{ab}_3\right) \ , \tag{54}$$

and

$$\begin{aligned} E_1 &= \mathrm{diag}\left(D_{1,\mu}\right) \\ &\equiv \mathrm{diag}\underbrace{\left(D_{1,1}, D_{1,2}, \cdots, D_{1,4}\right)}_{4} \ , \end{aligned} \tag{55}$$

$$\begin{aligned} E_i &= \mathrm{diag}\left(D_{i,\mu\nu}\right) \\ &\equiv \mathrm{diag}\underbrace{\left(D_{i,12}, D_{i,13}, \cdots, D_{i,43}\right)}_{12}, \ (i = 2, 3) \ , \end{aligned} \tag{56}$$

where we define the operator D as the fermion bilinears,

$$\left(D^\dagger_{1,\mu}\right)^{ab} = \frac{1}{2}\eta_{\mu,x}\bar{\chi}^a_x\chi^b_{x+\hat{\mu}} \ , \quad \left(D_{1,\mu}\right)^{ab} = \frac{1}{2}\eta_{\mu,x}\bar{\chi}^a_{x+\hat{\mu}}\chi^b_x \ , \tag{57}$$

$$\left(D^\dagger_{2,\mu\nu}\right)^{ab} = \frac{ir}{2^3\sqrt{3}}\eta_{\mu\nu,x}\bar{\chi}^a_x\chi^b_{x+\hat{\mu}+\hat{\nu}} \ , \quad \left(D_{2,\mu\nu}\right)^{ab} = \frac{ir}{2^3\sqrt{3}}\eta_{\mu\nu,x}\bar{\chi}^a_{x+\hat{\mu}+\hat{\nu}}\chi^b_x \ , \tag{58}$$

$$\left(D^\dagger_{3,\mu\nu}\right)^{ab} = \frac{ir}{2^3\sqrt{3}}\eta_{\mu\nu,x+\hat{\nu}}\bar{\chi}^a_{x+\hat{\nu}}\chi^b_{x+\hat{\mu}} \ , \quad \left(D_{3,\mu\nu}\right)^{ab} = \frac{ir}{2^3\sqrt{3}}\eta_{\mu\nu,x+\hat{\nu}}\bar{\chi}^a_{x+\hat{\mu}}\chi^b_{x+\hat{\nu}} \ . \tag{59}$$

Here V_1 and E_1 are 4×4 diagonal matrices while V_i and E_i $(i = 2, 3)$ are 12×12 diagonal matrices. Now we have prepared to obtain $W(\Lambda)$. By using the relation $U^\dagger U = 1$, we obtain the Schwinger-Dyson equation,

$$\frac{\partial^2 Z_x}{\partial E^{ab}_{\alpha\beta} \partial \left(E^\dagger\right)^{bc}_{\beta\gamma}} = -\delta_{ca}\delta^{\alpha\gamma} Z_x \ . \tag{60}$$

W should be a function of a gauge-invariant quantities as follows.

$$\Lambda^{ab}_{\alpha\beta} = \frac{1}{N^2} \left(E^\dagger E\right)^{ab}_{\alpha\beta} \ . \tag{61}$$

We can solve the Schwinger-Dyson equation analytically and derive W as a function of Λ,

$$W(\Lambda) = \mathrm{Tr} \left[(1 - 4\Lambda)^{1/2} - 1 - \ln \left[\frac{1 + (1 - 4\Lambda)^{1/2}}{2} \right] \right] \ . \tag{62}$$

We here perform trace for colors and hopping spaces.

$$\sum_x W(\Lambda) = -\sum_x \left[(1 - 4\Lambda_x)^{1/2} - 1 - \ln \left[\frac{1 + (1 - 4\Lambda_x)^{1/2}}{2} \right] \right] \ . \tag{63}$$

Finally we obtain a concrete form of Λ as

$$\Lambda_x = \frac{1}{8} \left[\sum_\mu \mathcal{M}_x \mathcal{M}_{x+\hat{\mu}} + \frac{1}{3} \sum_{\mu \neq \nu} \mathcal{M}_{x+\hat{\mu}} \mathcal{M}_{x+\hat{\mu}+\hat{\nu}} \right] - \left(\frac{r}{2^3\sqrt{3}} \right)^2 \sum_{\mu \neq \nu} \left(\mathcal{M}_x \mathcal{M}_{x+\hat{\mu}+\hat{\nu}} + \mathcal{M}_{x+\hat{\nu}} \mathcal{M}_{x+\hat{\mu}} \right) \ . \tag{64}$$

The first and second terms correspond to contribution from $D_{1,\mu}, D^\dagger_{1,\mu}$, and the third and forth terms correspond to contribution from $D_{i,\mu}, D^\dagger_{i,\mu}$ $(i = 2, 3)$. Now we again set $r = 2\sqrt{2}$ to compare the result to that of the hopping parameter expansion in Sec. IV. We need to change the fermion measure to the meson-field measure as

$$\int \mathcal{D}\left[\chi, \bar{\chi}\right] = \int \mathcal{D}\mathcal{M} \exp \left[-N \sum_x \ln \mathcal{M}_x \right] \ . \tag{65}$$

Then the effective partition function for the meson field is given by

$$Z(J) = \int \mathcal{D}\mathcal{M} \exp \left[N \left(\sum_x J_x \mathcal{M}_x + S_{\text{eff}}(\mathcal{M}) \right) \right] \ , \tag{66}$$

$$S_{\text{eff}}(\mathcal{M}) = \sum_x \left(\hat{M} \mathcal{M}_x - \ln \mathcal{M}_x \right) + \sum_x W(\Lambda) \ , \tag{67}$$

where we denote $\hat{M}$ as the shifted mass parameter $\hat{M} = M + 2r$. The partition function with $J = 0$ in the large N limit is reduced to the integrant for the saddle-point values of the meson fields,

$$\begin{aligned} Z(J=0) &= \int \mathcal{D}\mathcal{M} \exp\left[N S_{\text{eff}}(\mathcal{M})\right] \\ &\sim \exp\left[N S_{\text{eff}}(\bar{\mathcal{M}})\right], \quad (N \to \infty) \ . \end{aligned} \tag{68}$$

Now we consider pion condensate. For now, we consider only scalar σ and pseudo-scalar π fields as

$$\bar{\mathcal{M}}_x = \sigma + i\epsilon_x \pi \ , \tag{69}$$

$$= \Sigma e^{i\epsilon_x \theta} \ . \tag{70}$$

By substituting this form of the meson field into the Eq. (67), we derive the effective action for the Σ and θ,

$$\begin{aligned} S_{\text{eff}}(\bar{\mathcal{M}}) &= \hat{M} \sum_x \Sigma \cos\theta - \sum_x \ln \Sigma \\ &\quad - \sum_x \left[\left(1 - 4 \cdot 2\Sigma^2 \sin^2\theta\right)^{1/2} - \ln \left[\frac{1 + \left(1 - 4 \cdot 2\Sigma^2 \sin^2\theta\right)^{1/2}}{2} \right] \right] \ . \end{aligned} \tag{71}$$

We ignore the irrelevant constant. From the translational invariance, we factorize the 4-dimensional volume V_4 from the effective action as $S_{\text{eff}}(\bar{M}) = -V_4 V_{\text{eff}}(\Sigma, \theta)$. Then the effective potential V_{eff} is given by

$$\begin{aligned} V_{\text{eff}}(\Sigma, \theta) &= -\hat{M}\Sigma \cos\theta + \ln \Sigma \\ &\quad + \left[\left(1 - 4 \cdot 2\Sigma^2 \sin^2\theta\right)^{1/2} - \ln \left[\frac{1 + \left(1 - 4 \cdot 2\Sigma^2 \sin^2\theta\right)^{1/2}}{2} \right] \right] \ . \end{aligned} \tag{72}$$

Now let us look into the vacuum structure of this effective potential by solving the saddle-point condition, which are given by

$$\frac{\partial V_{\text{eff}}(\Sigma, \theta)}{\partial \Sigma} = -\hat{M}\cos\theta + \frac{1}{\Sigma} - \frac{8\Sigma \sin^2\theta}{1 + \left(1 - 4 \cdot 2\Sigma^2 \sin^2\theta\right)^{1/2}} = 0 \ , \tag{73}$$

$$\frac{\partial V_{\text{eff}}(\Sigma, \theta)}{\partial \theta} = \Sigma \sin\theta \left[\hat{M} - \frac{8\Sigma \cos\theta}{1 + \left(1 - 4 \cdot 2\Sigma^2 \sin^2\theta\right)^{1/2}} \right] = 0 \ . \tag{74}$$

Here we find two types of solutions for these equations depending on whether θ is zero or nonzero: For a trivial solution $\theta = 0$, we have $\Sigma = 1/\hat{M}$. For $\theta \neq 0$, the stationary conditions are written as

$$\hat{M}\Sigma - \cos\theta = 0 \ , \tag{75}$$

$$1 - \frac{8\Sigma^2}{1 + \left(1 - 4 \cdot 2\Sigma^2 \sin^2\theta\right)^{1/2}} = 0 \ . \tag{76}$$

Then, we find a solution for $\theta \neq 0$ as

$$\Sigma = \bar{\Sigma} = \sqrt{\frac{1}{8 - \hat{M}^2}} \ , \tag{77}$$

$$\sin^2\theta = \sin^2\bar{\theta} = \frac{2(4 - \hat{M}^2)}{8 - \hat{M}^2} \ . \tag{78}$$

Now we need to figure out which solution is realized as the vacuum of the theory by comparing the potentials for the two solutions. We easily show for $\hat{M}^2 < 4$,

$$V_{\text{eff}}(1/\hat{M}, 0) - V_{\text{eff}}(\bar{\Sigma}, \bar{\theta}) > 0 \ . \tag{79}$$

while $V_{\text{eff}}(1/\hat{M}, 0) - V_{\text{eff}}(\bar{\Sigma}, \bar{\theta}) < 0$ for $\hat{M}^2 > 4$. Thus the vacuum of the strong-coupling QCD with the Hoelbling-type staggered-Wilson fermion is given by the following: For $\hat{M}^2 > 4$ or equivalently $M > -4\sqrt{2} + 2,\ M < -4\sqrt{2} - 2$, there is only the chiral condensate as

$$\frac{1}{N}\langle\bar{\chi}\chi\rangle = \Sigma\cos\theta \quad = \frac{1}{\hat{M}} \ , \tag{80}$$

$$\frac{1}{N}\langle\bar{\chi}i\epsilon_x\chi\rangle = \Sigma\sin\theta \quad = 0 \ . \tag{81}$$

For $\hat{M}^2 < 4$ or equivalently $-4\sqrt{2} - 2 < M < -4\sqrt{2} + 2$, there is pion condensate which breaks parity symmetry spontaneously.

$$\frac{1}{N}\langle\bar{\chi}\chi\rangle = \bar{\Sigma}\cos\bar{\theta} \quad = \frac{\hat{M}}{8 - \hat{M}^2} \ , \tag{82}$$

$$\frac{1}{N}\langle\bar{\chi}i\epsilon_x\chi\rangle = \bar{\Sigma}\sin\bar{\theta} \quad = \pm\frac{\sqrt{2(4 - \hat{M}^2)}}{8 - \hat{M}^2} \ . \tag{83}$$

The sign of the pion condensate Eq. (83) reflects the Z_2 parity symmetry of the theory. The critical mass parameter $M_c = -4\sqrt{2} \pm 2$ and the range for the Aoki phase $-4\sqrt{2} - 2 < M < -4\sqrt{2} + 2$ is consistent with those of the hopping parameter expansion shown below Eq. (30). These results strongly suggest the existence of the parity-broken phase in the

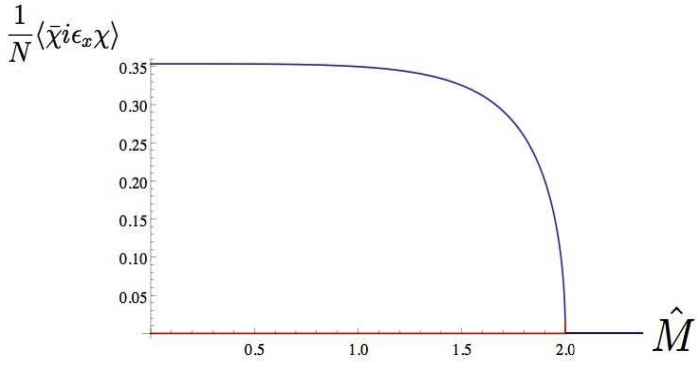

FIG. 8: The pion condensate undergoes second-order phase transition.

lattice QCD although it is just a strong-coupling limit. Figure 8 shows that the phase transition is second-order.

We can also derive mass spectrum of mesons by expanding the effective action Eq. (67) up to the quadratic terms of the meson-excitation field $\Pi_x = \mathcal{M}_x - \bar{\mathcal{M}}_x$. Since we are interested in the chiral limit which is taken from the parity-symmetric phase to the critical line, we here concentrate on the pion mass in the parity-symmetric phase. For the parity-symmetric phase ($\hat{M}^2 > 4$), the quadratic part of the effective action is given by

$$\begin{aligned} S_{\rm eff}(\mathcal{M}) - S_{\rm eff}(\bar{\mathcal{M}}) &= \sum_{x,y} S^{(2)}_{\rm eff}(x,y)\Pi_x\Pi_y \\ &= \int_{-\pi}^{\pi} \frac{d^4p}{(2\pi)^4}\Pi(-p)\mathcal{D}\Pi(p) \ , \end{aligned} \tag{84}$$

where $\Pi(p)$ is the Fourier component of Π_x, and

$$\mathcal{D} = \frac{1}{2\Sigma^2} + \left[\frac{1}{4}\sum_\mu \cos p_\mu - \frac{1}{24}\sum_{\mu\neq\nu}(\cos p_{\mu+\nu} + \cos p_{\mu-\nu})\right] \ , \tag{85}$$

with $p_{\mu\pm\nu} \equiv p_\mu \pm p_\nu$. Then we obtain the pion mass by solving $\mathcal{D} = 0$ at $p = (im_\pi a + \pi, \pi, \pi, \pi)$ as

$$\cosh(m_\pi a) = 1 + \frac{2\hat{M}^2 - 8}{3} \ . \tag{86}$$

By using the definition $K = 1/2\hat{M}$ with $\hat{M} = M + 2r$ and $r = 2\sqrt{2}$, we find $\cosh(m_\pi a) = 1 + (1 - 16K^2)/6K^2$, which is consistent with the result of the hopping parameter expansion

Eq. (35): The pion mass becomes zero at the critical mass $\hat{M}^2 = 4$, which indicates there occurs a second-order phase transition between parity-symmetric and broken phases in the strong-coupling limit. By defining quark mass as $m_q a = \hat{M} - \hat{M}_c$, we find PCAC relation near the critical mass as

$$(m_\pi a)^2 = \frac{16}{3} m_q a + \mathcal{O}(a^2) \ . \tag{87}$$

We can also study a case for non-zero spacial momenta by considering $p = (iEa + \pi, p_1 a + \pi, p_2 a + \pi, p_3 a + \pi)$ in Eq. (85). By using the pion mass Eq. (87) and re-normalizing the Dirac operator as $-\frac{8}{3}\mathcal{D} \to \mathcal{D}$, we show that Eq. (85) results in the Lorentz-covariant form up to $\mathcal{O}(a)$ discretization errors,

$$\mathcal{D} = (E^2 - \mathbf{p}^2 - m_\pi^2)a^2 + \mathcal{O}(a^3) \ , \tag{88}$$

with $\mathbf{p}^2 = p_1^2 + p_2^2 + p_3^2$. As we discussed in Sec. III, we expected that we may find a sign of Lorentz symmetry breaking of the Hoelbling fermion in this study. However, we eventually cannot find a disease due to the symmetry breaking in the strong-coupling study. We consider that it is because Lorentz symmetry breaking appears mainly in the gluon sector as shown in [28] and it is difficult to find it in the meson sector in this limit. In future work, we may be able to find it by including higher order corrections of $1/g^2$ and $1/N$.

We here discuss possibility of other condensation. For this purpose, we consider a general form of the meson field as

$$\bar{\mathcal{M}}_x = \sigma + i\epsilon_x \pi + \sum_\mu (-1)^{x_\mu} v_\mu + \sum_\mu i\epsilon_x (-1)^{x_\mu} a_\mu + \sum_{\mu>\nu} (-1)^{x_\mu + x_\nu} t_{\mu\nu} \ , \tag{89}$$

where we define the vector, axial-vector and tensor meson fields as v_μ, a_μ and t_μ. We can easily show there is no other condensate by substituting this general form Eq. (89) into the meson action Eq. (67). Thus we conclude that the vacuum we obtained is a true one.

The results in this section suggest that the chiral limit can be taken in Hoelbling-fermion lattice QCD in a parallel manner to Wilson fermion. However we probably need to tune other parameters to restore Lorentz symmetry in lattice QCD with this type. Therefore, what we can state here is just that, if we succeed to restore Lorentz symmetry by parameter tuning, this fermion could be applied to lattice QCD as Wilson fermion.

B. Adams type

We next investigate the case for the Adams fermion. We again consider the effective potential up to $\mathcal{O}(\mathcal{M}^3)$. The derivation is almost the same as the Hoelbling case in Subsec. V A. The main difference between them is the number of the multi-links. The fermion of the Adams type includes the four-hopping terms while the Hoelbling one has the two-hopping terms. In the appendix B, we derive the effective potential for the Adams-type fermion. Here we only summarize the results.

In this case, we again set $r = 16\sqrt{3}$ to match the result to that of the hopping parameter expansion in Sec. IV. We can derive the effective potential for scalar and pseudo-scalar fields by assuming condensation as $\mathcal{M}_x = \Sigma e^{i\epsilon_x\theta}$. We note that the functional form of the effective potential is the same as Eq. (72). By solving saddle-point equations, we find that the critical mass is given by $\hat{M}_c^2 = 4$ or equivalently $M_c = -16\sqrt{3} \pm 2$ with $\hat{M} = M + r$ and $r = 16\sqrt{3}$. The vacuum in this case is given by following: For $\hat{M}^2 > 4$ or $M > -16\sqrt{3} + 2$, $M < -16\sqrt{3} - 2$, there is only the chiral condensate as

$$\frac{1}{N}\langle\bar{\chi}\chi\rangle = \Sigma\cos\theta \quad = \frac{1}{\hat{M}} \ , \tag{90}$$

$$\frac{1}{N}\langle\bar{\chi}i\epsilon_x\chi\rangle = \Sigma\sin\theta \quad = 0 \ . \tag{91}$$

For $\hat{M}^2 < 4$ or $-16\sqrt{3} - 2 < M < -16\sqrt{3} + 2$, there emerge the pion condensate which breaks the parity symmetry spontaneously.

$$\frac{1}{N}\langle\bar{\chi}\chi\rangle = \bar{\Sigma}\cos\bar{\theta} \quad = \frac{\hat{M}}{8 - \hat{M}^2} \ , \tag{92}$$

$$\frac{1}{N}\langle\bar{\chi}i\epsilon_x\chi\rangle = \bar{\Sigma}\sin\bar{\theta} \quad = \pm\frac{\sqrt{2(4 - \hat{M}^2)}}{8 - \hat{M}^2} \ . \tag{93}$$

We note the critical mass and the parameter range of the Aoki phase are consistent with those of the hopping parameter expansion shown below Eq. (40). This result supports the existence of the parity-broken phase in the lattice QCD with the Adams fermion again. The behavior of pion condensate in this case is also given by Fig. 8, which shows the order of phase transition is second-order. This is consistent with the second-order scenario that we can take a chiral limit by a mass parameter tuning.

We derive the pion mass from the quadratic parts of the effective potential in a parallel

way to the Hoelbling type. The pion mass for this case is given by

$$\cosh(m_\pi a) = 1 + \frac{2\hat{M}^2 - 8}{5} \ , \tag{94}$$

for the parity-symmetric phase ($\hat{M}^2 > 4$). By using the definition $K = 1/2\hat{M}$ with $\hat{M} = M + r$ and $r = 16\sqrt{3}$, we find $\cosh(m_\pi a) = 1 + (1 - 16K^2)/10K^2$ which is consistent with the result of the hopping parameter expansion Eq. (45): The pion mass becomes zero at the critical mass $\hat{M}^2 = 4$, which indicates there occurs a second-order phase transition between parity-symmetric and broken phases in the strong-coupling limit. The PCAC relation holds near the critical mass also in this case.

$$(m_\pi a)^2 = \frac{16}{5} m_q a + \mathcal{O}(a^2) \ . \tag{95}$$

We can also show that the Lorentz-covariant dispersion relation recovers in the continuum limit in the Adams-type formalism as $\mathcal{D} = (E^2 - \mathbf{p}^2 - m_\pi^2)a^2 + \mathcal{O}(a^3)$. It is reasonable that Lorentz-symmetric dispersion recovers since Adams fermion has sufficiently large discrete symmetry for Lorentz symmetry restoration. We can also argue the possibility of other condensations in the same way: We can show there is no other condensates by substituting a general form of the meson fields (89) into the mesonic action for this case.

All these results indicate that, in Adams-type staggered-Wilson, we can take a chiral limit by tuning a mass parameter toward the second-order critical line from the parity-symmetric phase. Since Adams fermion has sufficient discrete symmetry, it can be straightforwardly applied to lattice QCD in a parallel manner to Wilson fermions.

VI. DISCUSSION ON TWO-FLAVOR CASE

In this section, we discuss parity-flavor breaking for two-flavor staggered-Wilson fermions. We first consider two-flavor Hoelbling-type fermion action. In this case, except that the low discrete symmetry would require further parameter tuning, the situation is quite similar to that of the Wilson fermion [12]. We here assume that mass parameters for two flavors M_f ($f = 1, 2$) are equal, which means there is exact $SU(2)$ flavor symmetry. The chiral and pion condensates are given by

$$\frac{1}{N}\langle \bar{\chi}_f \chi_f \rangle = \Sigma_f \cos\theta_f = \frac{1}{\hat{M}_f} \ , \tag{96}$$

$$\frac{1}{N}\langle \bar{\chi}_f i\epsilon_x \chi_f \rangle = \Sigma_f \sin\theta_f = 0 \ , \tag{97}$$

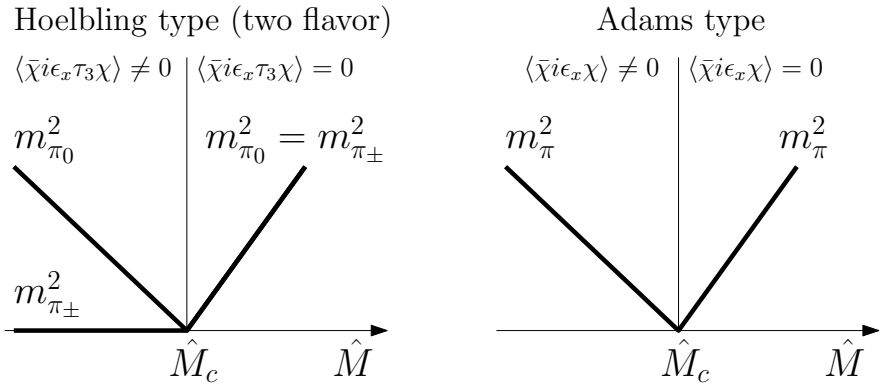

FIG. 9: Conjectures of pion mass behaviors as a function of a mass parameter in two-flavor Hoelbling fermions and a single Adams fermion. In both cases PCAC relation holds in the parity symmetric phase.

for $\hat{M}_f^2 \geq 4$ (parity-symmetric phase), while they are given by

$$\frac{1}{N}\langle\bar{\chi}_f\chi_f\rangle = \bar{\Sigma}_f \cos\bar{\theta}_f = \frac{\hat{M}_f}{8-\hat{M}_f^2} \ , \tag{98}$$

$$\frac{1}{N}\langle\bar{\chi}_f i\epsilon_x\chi_f\rangle = \bar{\Sigma}_f \sin\bar{\theta}_f = \pm\frac{\sqrt{2(4-\hat{M}_f^2)}}{8-\hat{M}_f^2} \ , \tag{99}$$

for $\hat{M_f}^2 < 4$ (Aoki phase). Here we have assumed that only the diagonal condensates in the flavor space (*i.e.* neutral condensates) can take finite values. Here we remind you of $\hat{M}_f = M_f + 2r$ with $r = 2\sqrt{2}$. We first look into the parity-symmetric phase. Although $SU(2)$ chiral symmetry is explicitly broken due to the flavored-mass term, three-massless pions appear on the second-order phase boundary due to divergence of correlation length as shown in Fig. 9. In the parity-broken phase, things depend on whether or not $\bar{\theta}_1$ and $\bar{\theta}_2$ have the same sign in Eq. (99). For $\bar{\theta}_1 = \bar{\theta}_2$,

$$\begin{aligned} &\langle\bar{\chi}i\epsilon_x\chi\rangle \neq 0 \ , \\ &\langle\bar{\chi}i\epsilon_x\tau_i\chi\rangle = 0 \ , \quad (i=1,2,3) \ , \end{aligned} \tag{100}$$

where τ_i is the Pauli matrix and χ stands a doublet $\chi = (\chi_1, \chi_2)^T$. For $\bar{\theta}_1 = -\bar{\theta}_2$,

$$\begin{aligned}
&\langle \bar{\chi} i\epsilon_x \chi \rangle = 0 \ , \\
&\langle \bar{\chi} i\epsilon_x \tau_1 \chi \rangle = 0 \ , \\
&\langle \bar{\chi} i\epsilon_x \tau_2 \chi \rangle = 0 \ , \\
&\langle \bar{\chi} i\epsilon_x \tau_3 \chi \rangle \neq 0 \ .
\end{aligned} \tag{101}$$

From Vafa-Witten's theorem [30], we expect that the latter vacuum ($\bar{\theta}_1 = -\bar{\theta}_2$) realizes [16]. It is also possible to check this by studying next-leading-order calculation of $1/N$ or $1/g^2$ expansions. If the latter scenario realizes, the flavored pion condensate Eq. (101) breaks $SU(2)$ flavor symmetry into its $U(1)$ subgroup as well as parity symmetry [32]. Thus, in the parity-broken phase, we have two-massless pions as NG bosons associated with spontaneous breaking of the flavor symmetry. We summarize them in Fig. 9. This situation is qualitatively the same as the case of Wilson fermion [12] except possibility of further parameter tuning to recover Lorentz symmetry.

The Adams-type staggered-Wilson fermion is more fascinating. It has two flavors for each branch in the first place. In this case there is no exact $SU(2)$ flavor symmetry due to taste-mixing in original staggered fermions. It means that in the parity-broken phase there is no massless excitation since there is no continuous symmetry to be broken as Fig. 9. However the number of massless pions in the chiral limit (on the boundary) depends on residual discrete flavor symmetry in the pion sector. If the discrete flavor symmetry is not sufficient to have a degenerate pion triplet, we have only one massless pion in the chiral limit although these three are expected to be degenerate in the continuum limit. If the symmetry is large enough, we have three-massless pions on the phase boundary. The latter is a quite fascinating scenario because we can simulate two-flavor QCD with a single lattice fermion. It is possible to study it by looking into transfer matrix symmetry or chiral Lagrangian potential. Recently Ref. [28] has reported that classification of pion operators from the transfer matrix symmetry indicates three-degenerate pions. Adams fermion can be a new standard of lattice fermion in the near future.

VII. SUMMARY AND DISCUSSION

In this paper we investigate strong-coupling lattice QCD with staggered-Wilson fermions, with emphasis on the parity-broken phase (Aoki phase) structure. We consider hopping parameter expansion and effective potential analysis in the strong-coupling limit. We have shown that the parity-broken phase and the second-order phase boundary exist for both Adams-type and Hoelbling-type staggered-Wilson fermions, which is consistent with the second-order scenario for a chiral limit.

In Sec. III, we discuss and classify discrete symmetries of two types of staggered-Wilson fermions. We show that they are invariant under charge conjugation and parity transformation, the latter of which is defined as 4th-shift followed by spatial axis reversal. We also discuss smaller rotation symmetry in the Hoelbling fermion, which would require further parameter tuning as shown in [28].

In Sec. IV, we analyze staggered-Wilson fermions by using hopping parameter expansion. From one-point functions of meson fields in the expansion, we find that pion condensate becomes nonzero in some range of the hopping parameter. From two-point functions, we show that square pion mass becomes zero on the boundary and becomes negative in the parameter region with nonzero pion condensate. These results suggest that there is a parity-broken phase and a second-order phase boundary.

In Sec. V, we study the effective potential for meson fields in the strong-coupling limit and large N limit to elaborate the phase structure in details. Here we develop a method to derive effective potential for lattice fermion actions with multiple-hopping terms. The gap equations from the effective potential exhibit nonzero pion condensate in the same parameter range as the hopping parameter expansion. From this analysis, we also show that pion becomes massless on the second-order phase boundary, and PCAC relation is reproduced around the boundary. If this property carries over into the weak-coupling regime, we can take a chiral limit by tuning a mass parameter in lattice QCD with staggered-Wilson fermions as with Wilson fermion.

In Sec. VI, we discuss the two-flavor cases. The situation in two-flavor Hoelbling-type fermions is similar to the original Wilson fermion except less rotational symmetry: Three-massless pions are expected to appear on the second-order critical lines, while two of them remain massless in the Aoki phase due to the flavored pion condensate. However we probably

need to care about Lorentz symmetry breaking in this case, thus we cannot straightforwardly apply it to two-flavor lattice QCD. The Adams-type staggered-Wilson fermion contains two flavors in each branch. Although the taste-mixing breaks flavor symmetry at finite lattice spacing, it does not necessarily mean non-degenerate three pions. Moreover SU(2) flavor symmetry should recover in the continuum limit at least, and three-massless pions emerge if we take a chiral and continuum limit. In this case, there is no rotational symmetry breaking, and the hypercubic symmetry will recover in the continuum limit. We can thus perform two-flavor QCD simulations with Adams-type staggered-Wilson fermion more efficiently than usual.

All of these results shows new possibilities of lattice fermion formulations. In particular, the Adams fermion can be straightforwardly applied to 2-flavor lattice QCD since it does not require any other fine-tuning and automatically has two flavors. Taking account of less numerical expenses in the staggered fermion, there is possibility that it would be numerically better than Wilson fermions, especially as an overlap kernel [11]. We finally note that the analysis here does not include contribution from some of higher-hopping terms or higher-meson fields. To confirm our results, we need to perform the same analysis with these higher contributions. In the future work, we can also study detailed mass spectrum of mesons and possibility of small other condensation in the Aoki phase.

Acknowledgments

TM is thankful to D. Adams, M. Creutz, M. Golterman, T. Izubuchi and S. Sharpe for the fruitful discussions. We are thankful to P. de Forcrand for the fruitful discussions. TK and TN are supported by Grants-in-Aid for the Japan Society for Promotion of Science (JSPS) Research Fellows (Nos. 22-3314, 23-593.). TM is supported by Grant-in-Aid for the Japan Society for Promotion of Science (JSPS) Postdoctoral Fellows for Reseach Abroad (24-8). This work is suppported in part by the Grants-in-Aid for Scientific Research from JSPS (Nos. 09J01226, 10J03314, 11J00593, 23340067, 24340054, and 24540271.), and by the Grant-in-Aid for the global COE program "The Next Generation of Physics, Spun from Universality and Emergence" from MEXT. This work is based on fruitful discussions in the YIPQS-HPCI workshop "New-Type of Fermions on the Lattice", Feb. 9-24, 2012 in Yukawa Institute for Theoretical Physics. The authors are grateful to the organizers for giving them

chances to have interest in the present topics.

Appendix A: spin and flavor separation

From one-staggered field we define 16 species fields in the momentum space as $\phi(p)_A \equiv \chi(p+\pi_A)$ $(-\pi/2 \le p_\mu < \pi/2)$ where π_A $(A = 1, 2, ..., 16)$ being 4-dim vectors whose components take 0 or π. For convenience, we here consider a 16-multiplet field as $\phi(p) = (\phi(p)_1, \phi(p)_2, \cdots, \phi(p)_{16})^T$. As this 16-multiplet field has both the spinor (space-time) and the flavor (taste) indices, we can construct two sets of clifford generators Γ_μ and Ξ_μ, which operate on spinor and flavor spaces in the momentum field $\phi(p)$. They satisfy the clifford algebra as

$$\{\Gamma_\mu, \Gamma_\nu\} = 2\delta_{\mu\nu} \ , \tag{A1}$$

$$\{\Xi_\mu, \Xi_\nu\} = 2\delta_{\mu\nu} \ , \tag{A2}$$

$$\{\Gamma_\mu, \Xi_\nu\} = 0 \ . \tag{A3}$$

By using these definitions, the Dirac operator for the staggered fermion is given by $D_{st} = i\Gamma_\mu \sin p_\mu$ for the 16 multiplet $\phi(p)$ [33].

Appendix B: Strong-coupling analysis for Adams-type

In this chapter, we show the derivation of the effective potential for the Adams-type fermion in the strong-coupling limit. To derive the effective potential for the Adams type, we replace Eq. (49) by Eq. (B1) in the Adams type.

$$\exp\left[\sum_x NW(\Lambda)\right] = \prod_x Z_x,$$

$$Z_x = \int \left(\prod_{\mu\neq\nu\neq\rho\neq\sigma} \mathcal{D}\left[U_{\mu,x}, U_{\mu,x+\hat{\nu}}, U_{\rho,x+\hat{\mu}+\hat{\nu}}, U_{\sigma,x+\hat{\mu}+\hat{\nu}+\hat{\rho}}\right] \right) \exp\left[-\left(\mathrm{Tr}(VE^\dagger) - \mathrm{Tr}(V^\dagger E) \right) \right] \ . \tag{B1}$$

Here we represent the partition function as 4 link integrals with $U_{\mu,x}$, $U_{\nu,x+\hat{\mu}}$, $U_{\rho,x+\hat{\mu}+\hat{\nu}}$, $U_{\sigma,x+\hat{\mu}+\hat{\nu}+\hat{\rho}}$. V and E in Eq. (B1) are the matrices which include components corresponding to 1-, 2-, 3-, and 4-link terms. The components of V and E consist of link variables and

TABLE III: Concrete forms of $\mathcal{W}^{(4)}_{\alpha\mu\beta\nu\gamma\rho\delta\sigma,x}$ in Fig. 4.

α	β	γ	δ	$\mathcal{W}^{(4)}_{\alpha\mu\beta\nu\gamma\rho\delta\sigma,x}$
+	+	+	+	$U_{\mu,x}U_{\nu,x+\hat{\mu}}U_{\rho,x+\hat{\mu}+\hat{\nu}}U_{\sigma,x+\hat{\mu}+\hat{\nu}+\hat{\rho}}$
−	−	−	−	$U^{\dagger}_{\mu,x-\hat{\mu}}U^{\dagger}_{\nu,x-\hat{\mu}-\hat{\nu}}U^{\dagger}_{\rho,x-\hat{\mu}-\hat{\nu}-\hat{\rho}}U^{\dagger}_{\sigma,x-\hat{\mu}-\hat{\nu}-\hat{\rho}-\hat{\sigma}}$
−	+	+	+	$U^{\dagger}_{\mu,x-\hat{\mu}}U_{\nu,x-\hat{\mu}}U_{\rho,x-\hat{\mu}+\hat{\nu}}U_{\sigma,x-\hat{\mu}+\hat{\nu}+\hat{\rho}}$
+	−	−	−	$U_{\mu,x}U^{\dagger}_{\nu,x+\hat{\mu}-\hat{\nu}}U^{\dagger}_{\rho,x+\hat{\mu}-\hat{\nu}-\hat{\rho}}U^{\dagger}_{\sigma,x+\hat{\mu}-\hat{\nu}-\hat{\rho}-\hat{\sigma}}$
+	−	+	+	$U_{\mu,x}U^{\dagger}_{\nu,x+\hat{\mu}-\hat{\nu}}U_{\rho,x+\hat{\mu}-\hat{\nu}}U_{\sigma,x+\hat{\mu}-\hat{\nu}+\hat{\rho}}$
−	+	−	−	$U^{\dagger}_{\mu,x-\hat{\mu}}U_{\nu,x-\hat{\mu}}U^{\dagger}_{\rho,x-\hat{\mu}+\hat{\nu}-\hat{\rho}}U^{\dagger}_{\sigma,x-\hat{\mu}+\hat{\nu}-\hat{\rho}-\hat{\sigma}}$
+	+	−	+	$U_{\mu,x}U_{\nu,x+\hat{\mu}}U^{\dagger}_{\rho,x+\hat{\mu}+\hat{\nu}-\hat{\rho}}U_{\sigma,x+\hat{\mu}+\hat{\nu}-\hat{\rho}}$
−	−	+	−	$U^{\dagger}_{\mu,x-\hat{\mu}}U^{\dagger}_{\nu,x-\hat{\mu}-\hat{\nu}}U_{\rho,x-\hat{\mu}-\hat{\nu}}U^{\dagger}_{\sigma,x-\hat{\mu}-\hat{\nu}+\hat{\rho}-\hat{\sigma}}$
+	+	+	−	$U_{\mu,x}U_{\nu,x+\hat{\mu}}U_{\rho,x+\hat{\mu}+\hat{\nu}}U^{\dagger}_{\sigma,x+\hat{\mu}+\hat{\nu}+\hat{\rho}-\hat{\sigma}}$
−	−	−	+	$U^{\dagger}_{\mu,x-\hat{\mu}}U^{\dagger}_{\nu,x-\hat{\mu}-\hat{\nu}}U^{\dagger}_{\rho,x-\hat{\mu}-\hat{\nu}-\hat{\rho}}U_{\sigma,x-\hat{\mu}-\hat{\nu}-\hat{\rho}}$
+	+	−	−	$U_{\mu,x}U_{\nu,x+\hat{\mu}}U^{\dagger}_{\rho,x+\hat{\mu}+\hat{\nu}-\hat{\rho}}U^{\dagger}_{\sigma,x+\hat{\mu}+\hat{\nu}-\hat{\rho}-\hat{\sigma}}$
+	−	+	−	$U_{\mu,x}U^{\dagger}_{\nu,x+\hat{\mu}-\hat{\nu}}U_{\rho,x+\hat{\mu}-\hat{\nu}}U^{\dagger}_{\sigma,x+\hat{\mu}-\hat{\nu}+\hat{\rho}-\hat{\sigma}}$
+	−	−	+	$U_{\mu,x}U^{\dagger}_{\nu,x+\hat{\mu}-\hat{\nu}}U^{\dagger}_{\rho,x+\hat{\mu}-\hat{\nu}-\hat{\rho}}U_{\sigma,x+\hat{\mu}-\hat{\nu}-\hat{\rho}}$
−	+	+	−	$U^{\dagger}_{\mu,x-\hat{\mu}}U_{\nu,x-\hat{\mu}}U_{\rho,x-\hat{\mu}+\hat{\nu}}U^{\dagger}_{\sigma,x-\hat{\mu}+\hat{\nu}+\hat{\rho}-\hat{\sigma}}$
−	−	+	+	$U^{\dagger}_{\mu,x-\hat{\mu}}U^{\dagger}_{\nu,x-\hat{\mu}-\hat{\nu}}U_{\rho,x-\hat{\mu}-\hat{\nu}}U_{\sigma,x-\hat{\mu}-\hat{\nu}+\hat{\rho}}$
−	+	−	+	$U^{\dagger}_{\mu,x-\hat{\mu}}U_{\nu,x-\hat{\mu}}U^{\dagger}_{\rho,x-\hat{\mu}+\hat{\nu}-\hat{\rho}}U_{\sigma,x-\hat{\mu}+\hat{\nu}-\hat{\rho}}$

fermion fields respectively. The concrete forms of the V and E for this case are given by

$$V^{ab}_{\alpha\beta} = \mathrm{diag}\left(V^{ab}_{1}, V^{ab}_{2}, \cdots, V^{ab}_{11}\right) \ , \tag{B2}$$

with

$$V_1 = \mathrm{diag}\left(U_{\mu,x}\right) \ , \tag{B3}$$

$$V_2 = \mathrm{diag}\left(U_{\mu,x}U_{\nu,x+\hat{\mu}}U_{\rho,x+\hat{\mu}+\hat{\nu}}U_{\sigma,x+\hat{\mu}+\hat{\nu}+\hat{\rho}}\right) \ , \tag{B4}$$

$$V_3 = \mathrm{diag}\left(U^{\dagger}_{\mu,x}U_{\nu,x}U_{\rho,x+\hat{\nu}}U_{\sigma,x+\hat{\nu}+\hat{\rho}}\right) \ , \tag{B5}$$

$$V_4 = \mathrm{diag}\left(U_{\mu,x+\hat{\nu}}U^{\dagger}_{\nu,x+\hat{\mu}}U_{\rho,x+\hat{\mu}}U_{\sigma,x+\hat{\mu}+\hat{\rho}}\right) \ , \tag{B6}$$

$$V_5 = \mathrm{diag}\left(U_{\mu,x+\hat{\rho}}U_{\nu,x+\hat{\mu}+\hat{\rho}}U^{\dagger}_{\rho,x+\hat{\mu}+\hat{\nu}}U_{\sigma,x+\hat{\mu}+\hat{\nu}}\right) \ , \tag{B7}$$

$$V_6 = \mathrm{diag}\left(U_{\mu,x+\hat{\sigma}}U_{\nu,x+\hat{\mu}+\hat{\sigma}}U_{\rho,x+\hat{\mu}+\hat{\nu}+\hat{\sigma}}U^{\dagger}_{\sigma,x+\hat{\mu}+\hat{\nu}+\hat{\rho}}\right) \ , \tag{B8}$$

$$V_7 = \mathrm{diag}\left(U_{\mu,x+\hat{\rho}+\hat{\sigma}}U_{\nu,x+\hat{\mu}+\hat{\rho}+\hat{\sigma}}U^{\dagger}_{\rho,x+\hat{\mu}+\hat{\nu}+\hat{\sigma}}U^{\dagger}_{\sigma,x+\hat{\mu}+\hat{\nu}}\right) \ , \tag{B9}$$

$$V_8 = \mathrm{diag}\left(U_{\mu,x+\hat{\nu}+\hat{\sigma}}U^{\dagger}_{\nu,x+\hat{\mu}+\hat{\sigma}}U_{\rho,x+\hat{\mu}+\hat{\sigma}}U^{\dagger}_{\sigma,x+\hat{\mu}+\hat{\rho}}\right) \ , \tag{B10}$$

$$V_9 = \mathrm{diag}\left(U_{\mu,x+\hat{\nu}+\hat{\rho}}U^{\dagger}_{\nu,x+\hat{\mu}+\hat{\rho}}U^{\dagger}_{\rho,x+\hat{\mu}}U_{\sigma,x+\hat{\mu}}\right) \ , \tag{B11}$$

$$V_{10} = \mathrm{diag}\left(U^{\dagger}_{\mu,x+\hat{\nu}}U^{\dagger}_{\nu,x}U_{\rho,x}U_{\sigma,x+\hat{\rho}}\right) \ , \tag{B12}$$

$$V_{11} = \mathrm{diag}\left(U^{\dagger}_{\mu,x+\hat{\rho}}U_{\nu,x+\hat{\rho}}U^{\dagger}_{\rho,x+\hat{\nu}}U_{\sigma,x+\hat{\nu}}\right) \ , \tag{B13}$$

$$E^{ab}_{\alpha\beta} = \mathrm{diag}\left(E^{ab}_1, E^{ab}_2, \cdots, E^{ab}_{11}\right) \ , \tag{B14}$$

and

$$E_1 = \mathrm{diag}\left(D_{1,\mu}\right) \ , \tag{B15}$$

$$E_i = \mathrm{diag}\left(D_{i,\mu\nu\rho\sigma}\right), \ (i = 2, 3, \cdots, 11) \ , \tag{B16}$$

where we define the operator D as the fermion bilinears,

$$\left(D^{\dagger}_{1,\mu}\right)^{ab} = \frac{1}{2}\eta_{\mu,x}\bar{\chi}^{a}_{x}\chi^{b}_{x+\hat{\mu}} \ , \quad (D_{1,\mu})^{ab} = \frac{1}{2}\eta_{\mu,x}\bar{\chi}^{a}_{x+\hat{\mu}}\chi^{b}_{x} \ , \tag{B17}$$

$$\left(D^{\dagger}_{2,\mu\nu\rho\sigma}\right)^{ab} = -s\bar{\chi}^{a}_{x}\chi^{b}_{x+\hat{\mu}+\hat{\nu}+\hat{\rho}+\hat{\sigma}} \ , \quad (D_{2,\mu\nu})^{ab} = s\bar{\chi}^{a}_{x+\hat{\mu}+\hat{\nu}+\hat{\rho}+\hat{\sigma}}\chi^{b}_{x} \ , \tag{B18}$$

$$\left(D^{\dagger}_{3,\mu\nu\rho\sigma}\right)^{ab} = -s_{\mu}\bar{\chi}^{a}_{x+\hat{\mu}}\chi^{b}_{x+\hat{\nu}+\hat{\rho}+\hat{\sigma}} \ , \quad (D_{3,\mu\nu})^{ab} = s_{\mu}\bar{\chi}^{a}_{x+\hat{\nu}+\hat{\rho}+\hat{\sigma}}\chi^{b}_{x+\hat{\mu}} \ , \tag{B19}$$

$$\left(D^{\dagger}_{4,\mu\nu\rho\sigma}\right)^{ab} = -s_{\nu}\bar{\chi}^{a}_{x+\hat{\nu}}\chi^{b}_{x+\hat{\mu}+\hat{\rho}+\hat{\sigma}} \ , \quad (D_{4,\mu\nu})^{ab} = s_{\nu}\bar{\chi}^{a}_{x+\hat{\mu}+\hat{\rho}+\hat{\sigma}}\chi^{b}_{x+\hat{\nu}} \ , \tag{B20}$$

$$\left(D^{\dagger}_{5,\mu\nu\rho\sigma}\right)^{ab} = -s_{\rho}\bar{\chi}^{a}_{x+\hat{\rho}}\chi^{b}_{x+\hat{\mu}+\hat{\nu}+\hat{\sigma}} \ , \quad (D_{5,\mu\nu})^{ab} = s_{\rho}\bar{\chi}^{a}_{x+\hat{\mu}+\hat{\nu}+\hat{\sigma}}\chi^{b}_{x+\hat{\rho}} \ , \tag{B21}$$

$$\left(D^{\dagger}_{6,\mu\nu\rho\sigma}\right)^{ab} = -s_{\sigma}\bar{\chi}^{a}_{x+\hat{\sigma}}\chi^{b}_{x+\hat{\mu}+\hat{\nu}+\hat{\rho}} \ , \quad (D_{6,\mu\nu})^{ab} = s_{\sigma}\bar{\chi}^{a}_{x+\hat{\mu}+\hat{\nu}+\hat{\rho}}\chi^{b}_{x+\hat{\sigma}} \ , \tag{B22}$$

$$\left(D^{\dagger}_{7,\mu\nu\rho\sigma}\right)^{ab} = -s_{\rho+\sigma}\bar{\chi}^{a}_{x+\hat{\rho}+\hat{\sigma}}\chi^{b}_{x+\hat{\mu}+\hat{\nu}} \ , \quad (D_{7,\mu\nu})^{ab} = s_{\rho+\sigma}\bar{\chi}^{a}_{x+\hat{\mu}+\hat{\nu}}\chi^{b}_{x+\hat{\rho}+\hat{\sigma}} \ , \tag{B23}$$

$$\left(D^{\dagger}_{8,\mu\nu\rho\sigma}\right)^{ab} = -s_{\hat{\nu}+\hat{\sigma}}\bar{\chi}^{a}_{x+\hat{\nu}+\hat{\sigma}}\chi^{b}_{x+\hat{\mu}+\hat{\rho}} \ , \quad (D_{8,\mu\nu})^{ab} = s_{\hat{\nu}+\hat{\sigma}}\bar{\chi}^{a}_{x+\hat{\mu}+\hat{\rho}}\chi^{b}_{x+\hat{\nu}+\hat{\sigma}} \ , \tag{B24}$$

$$\left(D^{\dagger}_{9,\mu\nu\rho\sigma}\right)^{ab} = -s_{\hat{\nu}+\hat{\rho}}\bar{\chi}^{a}_{x+\hat{\nu}+\hat{\rho}}\chi^{b}_{x+\hat{\mu}+\hat{\sigma}} \ , \quad (D_{9,\mu\nu})^{ab} = s_{\hat{\nu}+\hat{\rho}}\bar{\chi}^{a}_{x+\hat{\mu}+\hat{\sigma}}\chi^{b}_{x+\hat{\nu}+\hat{\rho}} \ , \tag{B25}$$

$$\left(D^{\dagger}_{10,\mu\nu\rho\sigma}\right)^{ab} = -s_{\hat{\mu}+\hat{\nu}}\bar{\chi}^{a}_{x+\hat{\mu}+\hat{\nu}}\chi^{b}_{x+\hat{\rho}+\hat{\sigma}} \ , \quad (D_{10,\mu\nu})^{ab} = s_{\hat{\mu}+\hat{\nu}}\bar{\chi}^{a}_{x+\hat{\rho}+\hat{\sigma}}\chi^{b}_{x+\hat{\mu}+\hat{\nu}} \ , \tag{B26}$$

$$\left(D^{\dagger}_{11,\mu\nu\rho\sigma}\right)^{ab} = -s_{\hat{\mu}+\hat{\rho}}\bar{\chi}^{a}_{x+\hat{\mu}+\hat{\rho}}\chi^{b}_{x+\hat{\nu}+\hat{\sigma}} \ , \quad (D_{11,\mu\nu})^{ab} = s_{\hat{\mu}+\hat{\rho}}\bar{\chi}^{a}_{x+\hat{\nu}+\hat{\sigma}}\chi^{b}_{x+\hat{\mu}+\hat{\rho}} \ . \tag{B27}$$

Note that $s = r\left(\epsilon\eta_5\right)_x/(4!\cdot 16)$, $s_\mu = r\left(\epsilon\eta_5\right)_{x+\hat{\mu}}/(4!\cdot 16)$, and $s_{\mu+\nu} = r\left(\epsilon\eta_5\right)_{x+\hat{\mu}+\hat{\nu}}/(4!\cdot 16)$. Here V_1 and E_1 are 4×4 diagonal matrices while V_i and E_i $(i = 2, 3, \cdots, 11)$ are 24×24 diagonal matrices. Here we note the situation of the cancellation between the diagrams crossing the different blocks is basically the same as the case for the Hoelbling type although there is difference between the 2-link and 4-link hoppings. We can derive W as a function of Λ by using the Schwinger-Dyson equation in a similar way to the Hoelbling type. Λ is

$$\begin{aligned}\Lambda_x = \frac{1}{16}\Bigg[&\sum_{\mu}\mathcal{M}_x\mathcal{M}_{x+\hat{\mu}} + \frac{1}{3}\sum_{\mu\neq\nu}\mathcal{M}_{x+\hat{\mu}}\mathcal{M}_{x+\hat{\mu}+\hat{\nu}} \\ &+ \frac{1}{6}\sum_{\mu\neq\nu\neq\rho}\mathcal{M}_{x+\hat{\mu}+\hat{\nu}}\mathcal{M}_{x+\hat{\mu}+\hat{\nu}+\hat{\rho}} + \frac{1}{6}\sum_{\mu\neq\nu\neq\rho\neq\sigma}\mathcal{M}_{x+\hat{\mu}+\hat{\nu}+\hat{\rho}}\mathcal{M}_{x+\hat{\mu}+\hat{\nu}+\hat{\rho}+\hat{\sigma}}\Bigg] \\ &- \left(\frac{r}{4!\cdot 16}\right)^2\sum_{\mu\neq\nu\neq\rho\neq\sigma}\left(2\mathcal{M}_x\mathcal{M}_{x+\hat{\mu}+\hat{\nu}+\hat{\rho}+\hat{\sigma}} + 4\mathcal{M}_{x+\hat{\mu}}\mathcal{M}_{x+\hat{\nu}+\hat{\rho}+\hat{\sigma}} + 2\mathcal{M}_{x+\hat{\mu}+\hat{\nu}}\mathcal{M}_{x+\hat{\rho}+\hat{\sigma}}\right) \ .\end{aligned} \tag{B28}$$

Appendix C: Order parameter and zero eigenvalue of staggered-Wilson operator

We investigate the relation between the order parameter $\langle\bar{\chi}i\epsilon_x\tau_3\chi\rangle$ for spontaneous symmetry breaking and zero eigenvalue of staggered-Wilson operator. In QCD, the chiral condensate $\langle\bar{\psi}\psi\rangle$ which is the order parameter for spontaneous breaking of chiral symmetry relates to the zero eigenvalue of Dirac operator. It is called Banks-Casher relation [31]. In Wilson fermion, the pion condensate $\langle\bar{\psi}i\gamma_5\tau_3\psi\rangle$ which is the order parameter for spontaneous breaking of parity-flavor symmetry relates to the zero eigenvalue of Wilson operator. In staggered-Wilson fermion (two-flavor Hoelbling type), we derive the relation between $\langle\bar{\chi}i\epsilon_x\tau_3\chi\rangle$ and zero eigenvalue as Wilson fermion. Then we add the external field H for order parameter to the Hoelbling-type staggered-Wilson action Eq. (12),

$$S_H(H) = \bar{\chi}\left[D_{SW}(M) + i\epsilon_x\tau_3 H\right]\chi \ . \tag{C1}$$

The order parameter $\langle\bar{\chi}i\epsilon_x\tau_3\chi\rangle$ is represented as,

$$\begin{aligned}
\lim_{H\to 0}\langle\bar{\chi}i\epsilon_x\tau_3\chi\rangle &= -\lim_{H\to 0}\lim_{V\to\infty}\frac{1}{V}\mathrm{Tr}\left(i\epsilon_x\tau_3\frac{1}{D_{SW}+i\epsilon_x\tau_3 H}\right)\\
&= -\lim_{H\to 0}\lim_{V\to\infty}\frac{1}{V}\mathrm{tr}\left[i\epsilon_x\left(\frac{1}{D_{SW}+i\epsilon_x H}-\frac{1}{D_{SW}-i\epsilon_x H}\right)\right]\\
&= -\lim_{H\to 0}\lim_{V\to\infty}\frac{1}{V}\mathrm{tr}\left[i\left(\frac{1}{H_{SW}+iH}-\frac{1}{H_{SW}-iH}\right)\right]\\
&= -i\lim_{H\to 0}\lim_{V\to\infty}\frac{1}{V}\sum_{\lambda}\langle\lambda\mid\left[\frac{1}{\lambda+iH}-\frac{1}{\lambda-iH}\right]\mid\lambda\rangle\\
&= -i\lim_{H\to 0}\lim_{V\to\infty}\frac{1}{V}\int d\lambda\rho\left(\lambda\right)\left[\frac{1}{\lambda+iH}-\frac{1}{\lambda-iH}\right]\\
&= -\frac{2\pi\rho(0)}{V}\\
&\equiv -\lim_{\epsilon\to 0}\lim_{H\to 0}\lim_{V\to\infty}\frac{2\pi\rho(\epsilon)}{V}\ ,
\end{aligned} \tag{C2}$$

where $H_{SW} = \epsilon_x D_{SW}$ is the Hermitian operator. Tr means the traces for flavor, color and space while tr means the traces for color and space. λ and $\mid\lambda\rangle$ are the eigenvalues and eigenstates and $\rho(\lambda) = \sum_{\lambda'}\delta(\lambda-\lambda')$ is the density of the state. By this analysis, we find the order parameter $\langle\bar{\chi}i\epsilon_x\tau_3\chi\rangle$ for spontaneous breaking of parity-flavor symmetry relates to the zero eigenvalue of the staggered-Wilson operator H_{SW}. Also, we can derive this relation

for Adams fermion in the same way.

---

[1] K. G. Wilson, Phys. Rev. D **10**, 2445 (1974).

[2] H. B. Nielsen and M. Ninomiya, Nucl. Phys. B **185**, 20 (1981); Nucl. Phys. B **193** 173 (1981); Phys. Lett. B **105** 219 (1981).

[3] M. Creutz, T. Kimura and T. Misumi, JHEP 1012, 041 (2010) [arXiv:1011.0761].

[4] T. Kimura, M. Creutz and T. Misumi, PoS Lattice2011 (2011) 106 [arXiv:1110.2482].

[5] J. B. Kogut and L. Susskind, Phys. Rev. D **11**, 395 (1975).

[6] L. Susskind, Phys. Rev. D **16**, 3031 (1977).

[7] H. S. Sharatchandra, H. J. Thun and P. Weisz, Nucl. Phys. B **192**, 205 (1981).

[8] D. H. Adams, Phys. Rev. Lett. **104**, 141602 (2010) [arXiv:0912.2850].

[9] D. H. Adams, Phys. Lett. B **699**, 394 (2011) [arXiv:1008.2833].

[10] C. Hoelbling, Phys. Lett. B **696**, 422 (2011) [arXiv:1009.5362].

[11] P. de Forcrand, A. Kurkela and M. Panero, PoS Lattice2010 (2011) 080 [arXiv:1102.1000]: JHEP **1204** (2012) 142 [arXiv:1202.1867].

[12] S. Aoki, Phys. Rev. D **30**, 2653 (1984).

[13] S. Aoki, Phys. Rev. D **33**, 2377 (1986); **34**, 3170 (1986); Phys. Rev. Lett. **57** 3136 (1986); Nucl. Phys. B **314**, 79 (1989).

[14] M. Creutz, (1996) [arXiv:hep-lat/9608024].

[15] S. Sharpe and R. Singleton. Jr, Phys. Rev. D **58**, 074501 (1998) [arXiv:hep-lat/9804028].

[16] Another interesting scenario is discussed in V. Azcoiti, G. Di Carlo, A. Vaquero, Phys. Rev. D **79**, 014509 (2009) [arXiv:0809.2972] and their other works.

[17] S. R. Sharpe, Phys. Rev. D **79**, 054503 (2009) [arXiv:0811.0409].

[18] P. H. Ginsparg and K. G. Wilson, Phys. Rev. D **25**, 2649 (1982).

[19] N. Neuberger, Phys. Lett. B **427**, 353 (1998) [arXiv:hep-lat/9801031].

[20] D. B. Kaplan, Phys. Lett. B **288**, 342 (1992) [arXiv:hep-lat/9206013].

[21] V. Furman and Y. Shamir, Nucl. Phys. B **439**, 54 (1995) [arXiv:hep-lat/9405004].

[22] M. Creutz, T. Kimura and T. Misumi, Phys. Rev. D **83**, 094506 (2011) [arXiv:1101.4239].

[23] T. Misumi, M. Creutz, T. Kimura, T. Z Nakano and A. Ohnishi, PoS Lattice2011 (2011) 108 [arXiv:1110.1231].

[24] N. Kawamoto and J. Smit, Nucl. Phys. B**192**, 100 (1981).

[25] C. van den Doel and J. Smit, Nucl. Phys. B **228**, 122 (1983).

[26] M. F. L. Golterman and J. Smit, Nucl. Phys. B **245**, 61 (1984).

[27] G. W. Kilcup and S. Sharpe, Nucl. Phys. B **283**, 493 (1987).

[28] S. Sharpe, Talk in YIPQS-HPCI workshop "New-Type of Fermions on the Lattice" (2012), http://www2.yukawa.kyoto-u.ac.jp/ws/2011/newtype/Talk-slides/sharpe-kyoto12-1.pdf and manuscript in preparation.

[29] T. Kimura, S. Komatsu, T. Misumi, T. Noumi, S. Torii and S. Aoki, JHEP **01 (2012)** 048 [arXiv:1111.0402].

[30] C. Vaffa and E. Witten, Phys. Rev. Lett **53**, 535 (1984).

[31] T. Banks and A. Casher, Nucl. Phys. B **169**, 103 (1980).

[32] In Appendix C, we show the relation between an order parameter of the phase transition and zero eigenvalues of staggered-Wilson operator, as Wilson fermion.

[33] The origin of the discrepancy between this form and the usual spin-taste representation is clearly elaborated in the reference, G. P. Lepage, [arXiv:1111.2955].